

## Flavien Paccot

LASMEA, UMR 6602 CNRS,  
Blaise Pascal University,  
Clermont-Ferrand, France  
flavien.paccot@lasmea.univ-bpclermont.fr

## Nicolas Andreff

LASMEA, UMR 6602 CNRS,  
Blaise Pascal University,  
Clermont-Ferrand, France  
and  
LAMI, IFMA, France

## Philippe Martinet

LASMEA, UMR 6602 CNRS,  
Blaise Pascal University,  
Clermont-Ferrand, France  
and  
ISRC, Sungkyunkwan University,  
Suwon, South Korea

# A Review on the Dynamic Control of Parallel Kinematic Machines: Theory and Experiments

## Abstract

*In this article, we review the dynamic control of parallel kinematic machines. It is shown that the classical control strategies from serial robotics generally used for parallel kinematic machine have to be rethought. Indeed, it is first shown that the joint space control is not relevant for these mechanisms for several reasons such as mechanical behavior or computational efficiency. Consequently, Cartesian space control should be preferred over joint space control. Nevertheless, some modifications to the well-known Cartesian space control strategies of serial robotics are proposed to make them perfectly suited to parallel kinematic machines, particularly a solution using an exteroceptive measure of the end-effector pose. The expected improvement in terms of accuracy, stability and robustness are discussed. A comparison between the main presented strategies is finally performed both in simulation and experiments.*

**KEY WORDS**—Parallel robot, motion control, dynamics

## Nomenclature

The general notation used in this article is as follows.

$X, \dot{X}, \ddot{X}$	Any representation of end-effector pose, velocity and acceleration
$q, \dot{q}, \ddot{q}$	Joint positions, velocities and accelerations
$FKM$	Forward kinematic model
$IKM$	Inverse kinematic model
$\dot{X} = D\dot{q}$	Forward instantaneous kinematics matrix, abusively called a Jacobian matrix
$\dot{q} = D_{inv}\dot{X}$	Inverse instantaneous kinematics matrix, abusively called an inverse Jacobian matrix
$\dot{D}$	Time derivative of the forward instantaneous kinematics matrix
$\dot{D}_{inv}$	Time derivative of the inverse instantaneous kinematics matrix
$FDM$	Forwards dynamic model
$IDM$	Inverse dynamic model
$\Gamma$	Actuation torques
$A$	Inertia matrix

---

The International Journal of Robotics Research  
Vol. 28, No. 3, March 2009, pp. 395–416  
DOI: 10.1177/0278364908096236  
©SAGE Publications 2009 Los Angeles, London, New Delhi and Singapore  
Figures 11, 14, 16–24 appear in color online: <http://ijr.sagepub.com>

$H$	Vector containing Coriolis, centrifugal and gravity forces
$M$	Inertia matrix of the actuated bodies, mapped into the active joint space, diagonal and constant
$I$	Inertia matrix of the end-effector, diagonal and constant
$\Gamma_f$	Friction forces
$F_v, F_s$	Viscous and dry friction parameters
$K_p, K_v, K_i$	Proportional, derivative and integral gain
$u_{PID}$	Signal generated by the PID controller
$u_{ff}$	Feedforward compensation term
$u_{comp}$	Compensation term
$v_d$	Desired variable $v$
$e = v_d - v$	Error signal between the desired and measured (or estimated) variable $v$
$s$	Laplace variable
$\hat{m}$	Numerical estimation of model $m$
$S(m)$	Skew matrix associated to the cross-product by vector $m$

**1. Introduction**

From a theoretical point of view, parallel kinematic machines allow for better dynamic performance than serial machines, in terms of speed, accuracy and stiffness (Merlet 2000). Therefore, they seem perfectly suitable for industrial high-speed applications, such as pick-and-place or high-speed machining. However, experiments on parallel kinematic machines point out that these good dynamic properties are not always established (Wang and Masory 1993; Tlusty et al. 1999; Pritschow 2002; Brecher et al. 2006a; Denkena and Holz 2006). Consequently, the improvement of static and dynamic accuracy is still an up-to-date and prosperous research field.

On the one hand, recent machines allow for impressive maximal acceleration, such as  $200 \text{ m s}^{-2}$  for the high-speed manipulator PAR4 (Nabat et al. 2005) or  $50 \text{ m s}^{-2}$  for the Urane SX machine tool (Company and Pierrot 2002). Such high acceleration cannot be achievable with serial kinematic machines. Consequently, the time gain is clearly established (Geldart et al. 2003; Terrier et al. 2004). On the other hand, several works deal with issues on the accuracy and stiffness of parallel kinematic machines. Pritschow (2002) presents a list of phenomena affecting the accuracy (see Figure 1). Two major issues are the object of numerous works.

The first major issue, the presence of numerous joints, causes kinematic model errors because of clearances and assembly defects (Wang and Masory 1993). Moreover, the com-

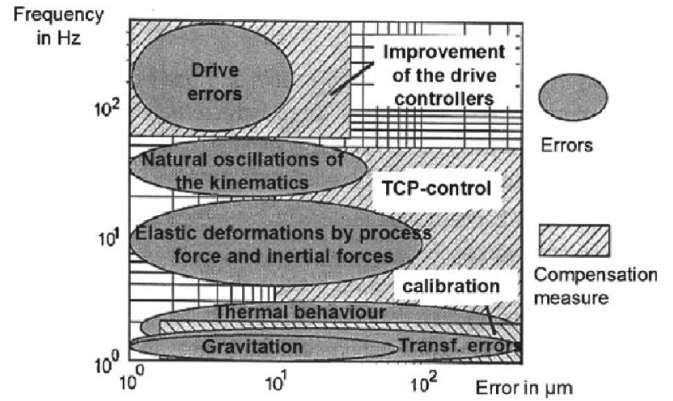


Fig. 1. Causes of the loss of accuracy according to Pritschow (2002).

plex kinematics often lead to model simplifications decreasing the accuracy (Pritschow 2002). The main solution to these problems is a performant kinematic identification (Wang and Masory 1993). It allows for matching as far as possible the machine model and its real behavior. The measures used for identification are performed with various means (Daney 1999; Besnard and Khalil 1999; Renaud et al. 2006; Chanal et al. 2006b). Another solution to kinematic errors consists of using adapted modeling methods to increase the model accuracy while simplifying the algorithms (Merlet 2000).

The second major issue, the actuators of a parallel kinematic machine tool, do not apply a torque along the end-effector motion axis, in contrast to a serial machine (Tlusty et al. 1999). It results in a decrease of stiffness leading to a lack of accuracy during the machining process. In this way, a workspace can be determined where stiffness allows for sufficient accuracy (Chanal et al. 2006a). Moreover, improvements are sought throughout the design of a new structure (Tlusty et al. 1999; Liu et al. 2000).

In summary, it seems that a parallel kinematic machine is really faster than a serial machine, but gains in terms of stiffness and accuracy are questionable. Actually, Merlet (2002) explains that the advantages of parallel kinematic machines can only be qualified as potential. To reach their theoretical performance, parallel kinematic machines still require improvements in design, modeling and control.

Nevertheless, the solutions presented above concern only mechanical design, kinematic modeling and identification. To our mind, the control of parallel kinematic machines is a field where great potential remains for improving accuracy. Indeed, most of the work in the literature only reuses the knowledge of serial robotics whereas control strategies have to be thought again to improve the performance of parallel kinematic machines. To illustrate this point, a state of the art on control is first presented in this paper, to point out the major issues that currently must be met. In this way, the relevant control

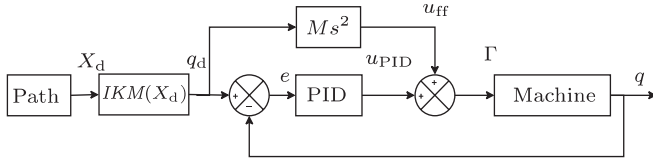


Fig. 2. Linear single-axis control with feedforward.

strategies are revisited and novel solutions are proposed, in the continuity of previous work (Ait Aider et al. 2006; Paccot et al. 2006, 2007). Then, the expected improvements from one control scheme to another are presented and discussed. Finally, some of the presented control strategies are applied to a specific test-bed. With the prerequisite of an adapted dynamic model and a dynamic identification, a comparison between the different control schemes is proposed with simulated and experimental results. Moreover, the comparison is achieved throughout realistic application and relevant measures.

This paper is organized as follows: Section 2 is devoted to the state of the art of joint space control, Section 3 concerns Cartesian space control and the proposed solutions, Section 4 deals with modeling the test-bed and Section 5 concerns the results.

## 2. Control of Parallel Kinematic Machines in the Joint Space

The knowledge of parallel robotics comes directly from serial robots. Therefore, parallel kinematic machines are mainly controlled with the same strategies as serial machines. Therefore, the main control methods met in the literature are linear single-axis and computed torque control, both in the joint space.

### 2.1. Linear Single-axis Control

In most industrial cases, a linear single-axis control, also called PID control or simple control, is used (Khalil and Dombre 2002; Zhiyong and Huang 2004; Brecher et al. 2006a; Denkena and Holz 2006; Yang and Huang 2006). Figure 2 displays this well-known control scheme. This is the conventional and simplest way to control a system. It can be used for serial and parallel kinematic machines. Therefore, controllers can be reused, from serial to parallel kinematic machines, without major adaptation, making this control strategy interesting in an industrial context. In addition, it provides rather good performance with regards to its wide use. The tuning of such a control is well known from the classical robotics method (Khalil and Dombre 2002) to more elaborated methods, adapted for parallel kinematic machines (Zhiyong and Huang 2004; Yang and Huang 2006).

Let us remind the reader of the conventional method for a theoretical tuning (Khalil and Dombre 2002). Out of habit, the assumption of simple dynamics only with inertia forces associated with a single constant and diagonal inertia matrix  $M$ , and without centrifugal, Coriolis and gravity forces is made:

$$\Gamma = M\ddot{q}. \quad (1)$$

The PID controller generates directly a torque input,  $u_{\text{PID}}$ :

$$u_{\text{PID}} = K_v \dot{e} + K_p e + K_i \int e dt. \quad (2)$$

The denominator of the closed loop transfer function can be thus expressed as

$$B(s) = (Ms^3 + K_v s^2 + K_p s + K_i) \quad (3)$$

The classical tuning aims at obtaining a third-order negative real poles system:

$$B(s) = M(s + \omega)^3 \quad (4)$$

with  $\omega$  chosen with respect to the mechanical resonance frequency of the controlled machine. By matching each term of (3) and (4), the gain values are expressed as follows:

$$\begin{cases} K_v = 3M\omega, \\ K_p = 3M\omega^2, \\ K_i = M\omega^3. \end{cases} \quad (5)$$

This tuning gives theoretical values which have to be adapted in practice. Indeed, the integral gain  $K_i$  is generally increased to compensate for the dry frictions, while the derivative gain  $K_v$  is generally decreased to cope with measurement noise.

In most cases, the linear single-axis control is improved with a feedforward term,  $u_{\text{ff}}$ . The general formulation of this term is

$$u_{\text{ff}} = M\ddot{q}_d. \quad (6)$$

In this case, the error signal behavior is fixed by a third-order ordinary differential equation:

$$Me^{(3)} + K_v \ddot{e} + K_p \dot{e} + K_i e = 0, \quad (7)$$

where  $e^{(3)}$  is the third derivative with respect to time.

The gain values are the same as (5), which allows for a performant error behavior. Let us notice that the  $M$  matrix is often used out of the feedforward and PID gain, as in Figure 3. It yields to the following error signal behavior:

$$M(e^{(3)} + K_v \ddot{e} + K_p \dot{e} + K_i e) = 0 \quad (8)$$

and a gain tuning independent from the machine inertia:

$$\begin{cases} K_v = 3\omega, \\ K_p = 3\omega^2, \\ K_i = \omega^3. \end{cases} \quad (9)$$

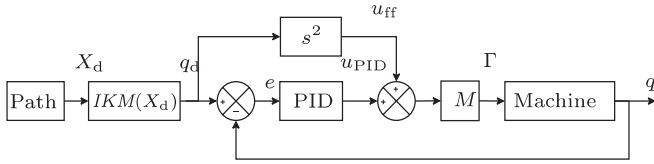


Fig. 3. Linear single-axis control with feedforward, practical version.

Furthermore, in an industrial controller, some additional features are used, such as friction, gravity and backlash compensation, to improve accuracy. Such a control strategy ensures sufficiently good performances for serial kinematic machine tools to make it still widely used in the industry. Nevertheless, a machine tool is quite slow, very heavy and stiff. Therefore, a single-axis linear control ensures an efficient compensation of the small dynamics and the behavior of the stiff mechanical structure ensures a good static accuracy.

On the other hand, the single-axis control is known to be weak with fast serial manipulators since it does not ensure a sufficient compensation of the non-linear dynamics, leading to a poor dynamic accuracy (Khalil and Dombre 2002). Actually, reported experiments show that such a control cannot ensure a good accuracy for parallel kinematic machines (Honegger et al. 2000; Ouyang et al. 2002; Vivas et al. 2003; Brecher et al. 2006a; Denkena and Holz 2006). Indeed, the presence of the complex inverse kinematics in the path planning is a first source of static accuracy lack, requiring adapted modeling and identification as stated above. However, the complex dynamic behavior is also a very unfavorable phenomenon.

As a matter of fact, the dynamic behavior of a parallel kinematic machine is strongly non-linear due to dynamic coupling between the legs, which does not exist in the serial case. Furthermore, most of the parallel kinematic machines have an anisotropic behavior. Therefore, the hypothesis of linear dynamics is only verified at low speed and very locally. Consequently, a linear single-axis control cannot be efficient in the whole workspace with the same tuning, as established by Brecher et al. (2006a). A first solution is the determination of a restricted workspace with regard to maximal accelerations, as initiated by Barrette and Gosselin (2005). This method could be extended with the determination of a workspace, associated with a maximal speed and acceleration, where dynamics are fairly homogeneous with a low dynamic coupling. A second method is path planning with dynamic consideration (Abdelatif and Heiman 2005; Oen and Wang 2007). In addition, the use of an adapted time interpolation can smooth the trajectory by limiting jerk or snap (respectively fourth- and fifth-order time derivative of the joint position) (Erkorkmaz and Altintas 2001; Fleisig and Spence 2001; Lambrechts et al. 2005). It should be noted that a feedforward compensation in terms of jerk and snap can thus be used (Lambrechts et al. 2005). Such methods aim to ease controller action to ensure the required

accuracy. However, the limitations of such methods are the decrease of the effective speed and workspace leading to a low use of the machines capabilities. Moreover, the real machine motion is not completely mastered since the heavy computation generally imposes an off-line path generation without any on-line corrections of this path.

To improve the real machine motion control, the control gain tuning can be optimized with dynamic considerations, as proposed by Zhiyong and Huang (2004) and Yang and Huang (2006). Other solutions consist in control laws modification (not always achievable on an industrial controller). Some works deal with non-linear gains (Ouyang et al. 2002), robust control (Kim et al. 2005; Fu and Mills 2005) and inappreciable phenomena compensation (Brecher et al. 2006b). Nevertheless, these strategies are still based on a single-axis control with various compensation in an external loop. There is no dynamics compensation in the control loop. However, a direct and simple way to compensate for the dynamic behavior is the well-known computed torque control.

### 2.2. Computed Torque Control

The computed torque control is a widespread control strategy for serial manipulators (Luh et al. 1980; Khalil and Dombre 2002). Figure 4 displays an example of this control scheme. Let us remind the reader of how the classical computed torque control works (Khalil and Dombre 2002). The control law is based on the Lagrange formulation of the machine inverse dynamic model:

$$\Gamma = A(q)\ddot{q} + H(q, \dot{q}). \tag{10}$$

By replacing  $\ddot{q}$  in (10) by an adapted control signal  $u$ , an exact linearization of the dynamics is ensured. Indeed, there is only a double integrator between control signal and joint variables. The following control signal is used:

$$u = \ddot{q}_d + K_v\dot{e} + K_d e. \tag{11}$$

In this case, the error signal has a second-order behavior:

$$\ddot{e} + K_v\dot{e} + K_d e = 0. \tag{12}$$

The gain tuning is, as is well known, fixed by a cut-off frequency and a damping:

$$\begin{cases} K_v = 2\zeta\omega, \\ K_d = \omega^2. \end{cases} \tag{13}$$

The damping  $\zeta$  is generally fixed between 0.9 and 1 to avoid overshoot while yielding a good establishing time. The cut-off frequency  $\omega$  is fixed to the highest value with respect to the mechanical resonance frequency. It should be noted that the integral gain is useless because the linearization of the dynamics leads to a double integrator system. However, the integral

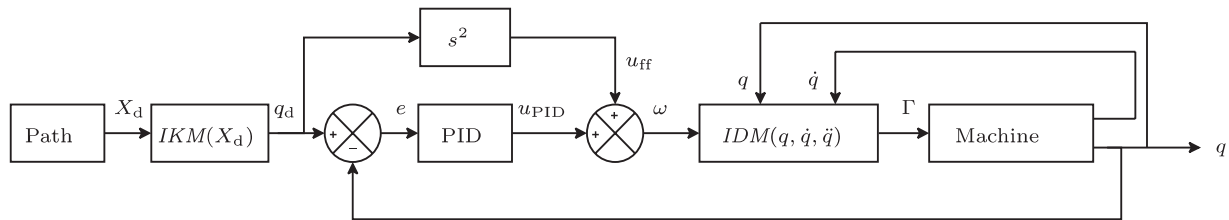


Fig. 4. Joint space computed torque control.

gain is generally employed in practice. It allows the accuracy to be improved by compensating for the light unmodeled phenomena. Nevertheless, this control strategy can be improved with friction and backlash compensation, in the same way as the linear single-axis control.

With such a control scheme, the non-linear dynamic behavior of the machine is compensated for in the whole workspace. In this way, the linear controller is associated with an exactly linearized system. Therefore, the controller performances are maximal and homogeneous in the whole workspace. Nevertheless, these great performances are only achievable with a dynamic model reflecting the real machine behavior perfectly. Indeed, the computed torque control does not cope very well with modeling errors (Khalil and Dombre 2002). They create a perturbation on the error behavior which may lead to a lack of stability and accuracy. Since a model almost never reflects the real machine behavior exactly, modeling errors are nearly unavoidable. Consequently, a minimization of these modeling errors is required. In this way, dynamic identification is generally performed (Swevers et al. 1997; Gautier and Poignet 2001; Olsen and Peterson 2001). Alternately, a more complex model can be used. A flexible body dynamic model (Kock and Shimacher 2000b), instead of a rigid body model, allows the deformations to be taken into account, increasing the accuracy of the model while increasing on-line computation. A model taking into account task influence (Oen and Wang 2007), instead of a model of the stand-alone mechanical structure, can cope with external torques applied on the end-effector, which are specific for the application (cutting, carrying a load, etc.). Furthermore, if the influence of the modeling errors is still interfering, robust control technique can be employed (Honegger et al. 2000; Lee et al. 2003; Vivas et al. 2003). Actually, robust techniques are used here to compensate for the phenomena which cannot be modeled, as they were originally designed for, and not to compensate for insufficient modelling, as is seen too often.

### 2.3. Discussion

The control strategies exposed above are performed in the joint space. Practically, the actuators' encoders are generally the

only available measurement mean. Theoretically, a serial kinematic machine is completely defined by its joint configuration, in terms of kinematics and dynamics (Khalil and Dombre 2002). The joint configuration thus reflects the state of the machine. Consequently, the joint space control is a state feedback control. As is generally admitted, a state feedback control allows the best accuracy to be obtained. Therefore, the joint space control is relevant for serial kinematic machine, provided that solving for the inverse kinematic problem is accurate enough to translate the desired Cartesian path into the correct joint reference path.

On the other hand, a parallel kinematic machine is completely defined by its end-effector pose, except in some rare cases (3RRR for example (Chablat and Wenger 1998)). Actually, this is generally admitted for the kinematics (Waldron and Hunt 1991; Merlet 2002; Dallej et al. 2006) and it is being extended to the dynamics (Dasgupta and Choudhury 1999; Khalil and Ibrahim 2004; Callegari et al. 2006). The end-effector pose can thus be considered as the state of a parallel kinematic machine (Dallej et al. 2006). Therefore, a joint space control is not a state feedback control but a biased observer feedback control. Consequently, the best performance in term of accuracy cannot be ensured with such a control.

Moreover, the instantaneous kinematics and dynamics depend on the end-effector pose as stated above. Consequently, a joint space model-based control, such as the computed torque control, should include the forward kinematic model. To illustrate this point, we propose an explicit form of the computed torque control in the joint space which includes these forward transformations (see Figure 5). In general, the forward kinematics of a parallel kinematic machine do not have a closed-form expression in contrast to a serial machine. A joint configuration can thus lead to several end-effector poses (namely up to 40 for the Gough–Stewart platform (Merlet 1990; Husty 1994)). Some solutions can be removed since they are complex or mechanically inadmissible, but the end-effector pose cannot be estimated only from the active joint configuration with reliability. Indeed, the forward kinematic problem is a square model since it has exactly the same amount of equations and unknowns. Hence, it is sensitive to any measurement noise, not even to mention the kinematic model and calibration errors. In addition, the on-line computation of the

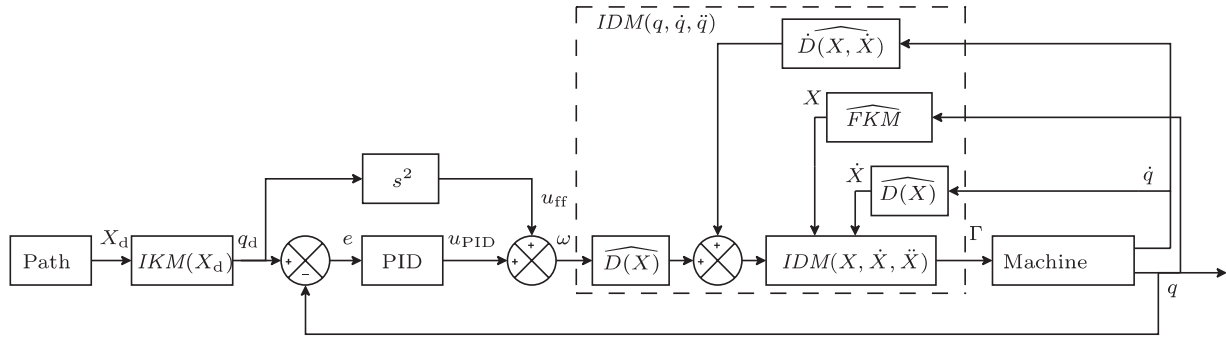


Fig. 5. Joint space computed torque control for a parallel kinematic machine, explicit version.

end-effector pose leads to a lack of speed, accuracy and stability. Consequently, the performances of the control are limited. Furthermore, the implicit presence of on-line numerical transformations leads, in practice, to model simplifications thus increasing modeling errors. As reminded above, the computed torque control has a weak robustness with regards to the modeling errors. Thus, the joint space computed torque control is often unusable by itself. Some solutions are reported such as simplified dynamics and robust control (Lee et al. 2003; Vivas et al. 2003) or non-linear feedforward compensation with robust control (Honegger et al. 2000). Nevertheless, the mastery of robust control and the perfectible accuracy make the joint space computed torque control unwelcome in an industrial context.

As a conclusion, the joint space control seems to be inherently imperfect and unadapted for parallel kinematic machines. Since the latter are completely defined by their end-effector pose, improvements could be found in the Cartesian space ( $SE_3$ ) control.

### 3. Control of the Parallel Kinematic Machines in the Cartesian Space

To the best of the authors' knowledge, the control of a parallel kinematic machine in the Cartesian space, or the task space, is often mentioned in the literature (Beji et al. 1998; Yamane et al. 1998; Kock and Shimacher 2000a; Marquet et al. 2001; Caccavale et al. 2003; Lee et al. 2003; Callegari et al. 2006). Nevertheless, only few experiments have been performed. When it is used, many model simplifications are performed decreasing the accuracy and stability (Lee et al. 2003). The purpose of this section, which is the essential theoretical contribution of this paper, is therefore to propose a complete revisiting of the Cartesian space control strategies. It is based on the serial-parallel duality (Waldron and Hunt 1991) and thus requires the following assumption.

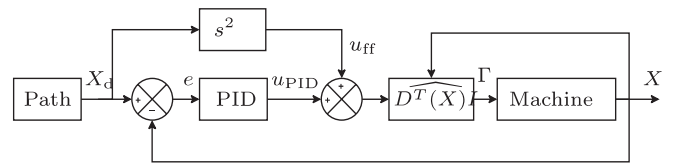


Fig. 6. Simple PID control in the Cartesian space, first version.

**Assumption 1.** The end-effector pose can be measured accurately at the control frequency.

This assumption is discussed in Section 3.3.

#### 3.1. Equivalent of Single-axis Linear Control in the Cartesian Space

##### 3.1.1. With the End-effector Dynamics Only

The Cartesian space equivalent of the linear single-axis control given by Figure 6 is generally used (Callegari et al. 2006). However, it is shown that the transposition from joint to Cartesian space is not completely straightforward. In the control scheme of Figure 6, the simplified dynamics is expressed as

$$\Gamma = \widehat{D}^T(X)I\ddot{X}, \tag{14}$$

where only the inertia of the end-effector  $I$  is taken into account. The latter is mapped into the active joint space with the forward instantaneous kinematic matrix.

The feedforward compensation term can be then expressed as

$$u_{ff} = \ddot{X}_d. \tag{15}$$

In this case, the error signal behavior is fixed by the following equation:

$$\widehat{D}^T(X)I(e^{(3)} + K_v\dot{e} + K_p e) = 0. \tag{16}$$

Consequently, the following tuning should be used:

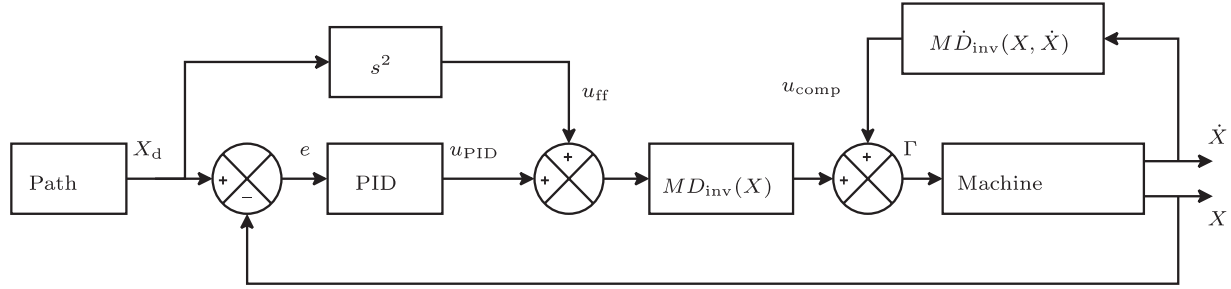


Fig. 7. Simple PID control in the Cartesian space, second version.

$$\begin{cases} K_v = 3\omega, \\ K_p = 3\omega^2, \\ K_i = \omega^3. \end{cases} \quad (17)$$

Consequently, a similar running between single-axis linear control and this Cartesian space control strategy is retrieved here, with similar dynamics, feedforward compensation term and PID tuning. The only difference is the presence of the transposed forward instantaneous kinematic matrix in the control loop. However, we can make some remarks here. First, the presence of a numerically estimated model in the control loop can lead to a lack of stability and accuracy, and increases the complexity of the control scheme. Second, the dynamics in (14) only concerns the end-effector inertia and the legs inertia is neglected. However, this assumption seems to be too restrictive, particularly in the machine-tool case where legs are generally heavier than the end-effector. The compensation of the machine dynamic behavior might not, hence, be achieved efficiently. Thus, the accuracy of this control strategy is questionable. Let us see whether it is more relevant to take into account the legs simplified dynamics.

### 3.1.2. With the Leg Dynamics Only

The simplified inverse dynamics in (1) is reused here. The joint acceleration  $\ddot{q}$  is expressed as a function of the end-effector pose with the second-order inverse instantaneous kinematics:

$$\Gamma = M (D_{inv}(X)\ddot{X}_d + \dot{D}_{inv}(X, \dot{X})\dot{X}_d). \quad (18)$$

The feedforward term is also expressed in as a function of the end-effector pose:

$$u_{ff} = M (D_{inv}(X)\ddot{X}_d + \dot{D}_{inv}(X, \dot{X})\dot{X}_d). \quad (19)$$

In this case, the error signal behavior is fixed by the following equation:

$$MD_{inv}(X)e^{(3)} + (K_v + M\dot{D}_{inv}(X, \dot{X}))\dot{e} + K_p\dot{e} + K_i e = 0. \quad (20)$$

Consequently, the following tuning has to be used:

$$\begin{cases} K_v = 3MD_{inv}(X)\omega - M\dot{D}_{inv}(X, \dot{X}), \\ K_p = 3MD_{inv}(X)\omega^2, \\ K_i = MD_{inv}(X)\omega^3. \end{cases} \quad (21)$$

In a first approach, with this formulation, the tuning is not constant and thus difficult to set up in an industrial context. Nevertheless, we can rearrange each term to propose a lighter control scheme, as illustrated by Figure 7. In this case, the feedforward term is

$$u_{ff} = \ddot{X}_d. \quad (22)$$

A compensation term is added. It is expressed as

$$u_{comp} = M\dot{D}_{inv}(X, \dot{X})\dot{X}. \quad (23)$$

In this case, the error signal behavior is fixed by the following equation:

$$MD_{inv}(X)(e^{(3)} + K_v\ddot{e} + K_p\dot{e} + K_i e) = 0. \quad (24)$$

Consequently, the gain tuning becomes

$$\begin{cases} K_v = 3\omega, \\ K_p = 3\omega^2, \\ K_i = \omega^3. \end{cases} \quad (25)$$

This proposed control strategy is the direct Cartesian space equivalent to the single-axis control in the joint space. However, it should be noted that the transposition between Cartesian and joint space is not as straightforward as it could have seemed at first glance. The control scheme complexity has clearly increased whereas the dynamics compensation issues listed previously are still present since the same simplified dynamics is used. Moreover, the end-effector dynamics is neglected.

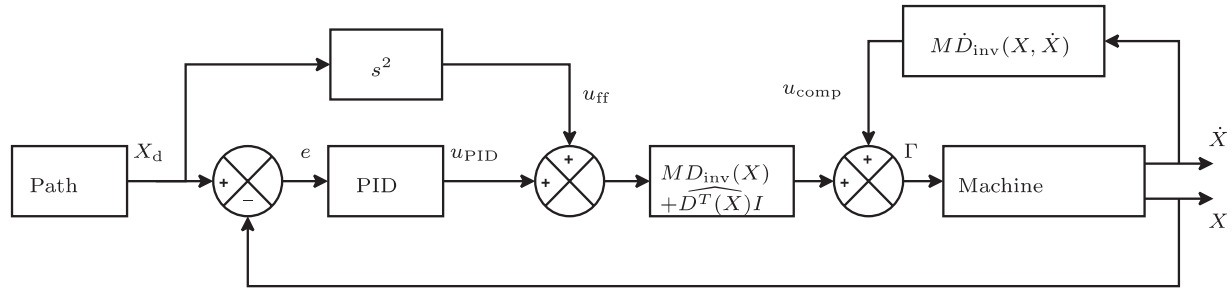


Fig. 8. Simple PID control in the Cartesian space, third version.

3.1.3. With the Legs and End-effector Dynamics

Now, the two simplified dynamics used above can be grouped together to take into account both legs and end-effector inertia (Figure 8). Thus, a more elaborated expression of the simplified dynamics can be

$$\Gamma = M\ddot{q} + D^T I \ddot{X}. \tag{26}$$

The control law is nearly the same as that presented above (compare Figure 7 and Figure 8). The tuning is the same as (25). Nevertheless, a more efficient compensation of the machine dynamic behavior can be performed here in comparison with the two previous cases (Sections 3.1.1 and 3.1.2) since more phenomena are taken into account. However, the numerical issues of the forward instantaneous kinematic matrix are retrieved here and thus impose some care.

Let us remark that this formulation is used by Marquet et al. (2001) and Vivas et al. (2003) directly in a computed torque control. Nevertheless, since these simplified dynamics presents inevitably important modeling errors, a predictive control, asking for heavy computation, is thus employed to ensure good performances at high speed. Actually, this approach stands on the border between simple control and computed torque control: the control is almost considered as a single-axis control when a simple PID controller is used, and as a computed torque control when a more complex controller is used.

Consequently, the interest of change from the joint to Cartesian space could be questionable, in the simple PID control case. Nevertheless, we show in Section 3.3 some mechanical advantages for the Cartesian space control. Now, instead of using simplified dynamics and time-consuming complex controller, the use of the complete dynamics in a computed torque control can allow for a simpler controller with lighter computational burden, while ensuring equivalent or better performances.

3.2. Computed Torque Control in the Cartesian Space

The Cartesian space computed torque control is well known for serial kinematic machines (Khalil and Dombre 2002). The

presence of the numerical inverse instantaneous kinematic matrix  $\widehat{D}_{inv}$  (see Figure 9) mean that this control strategy is rarely used for serial kinematic machines. Indeed, the forward instantaneous kinematic matrix of a serial kinematic machine is generally composed of trigonometric functions, thus making the numerical inversion all the more difficult because of the existence of numerous singularities and non-linear dependence upon noise.

On the other hand, in the parallel kinematic case, this control scheme is perfectly relevant when it encloses an inverse dynamic model depending on the end-effector pose and time derivatives (Caccavale et al. 2003; Callegari et al. 2006). Indeed, there is a minimal use of numerical transformations when the end-effector pose and speed are measured (see Figure 10). Actually, the only used numerical transformation is the transposed forward instantaneous kinematics matrix used to map the Cartesian space dynamics into the active joint space (Dasgupta and Choudhury 1999; Khalil and Ibrahim 2004; Callegari et al. 2006). Since inverting this matrix consists only of a numerical inversion of quite a simple matrix, the computational burden is less important than for solving for the forward kinematics problem. Moreover, the Cartesian space computed torque control for parallel kinematic machines is dual with the joint space computed torque control for the serial kinematic machines (see Figures 4 and 10). Consequently, the behavior of the joint space computed torque control described above is retrieved here, namely the error behavior in (12) and the tuning in (13), which we recall here:

$$\ddot{e} + K_v \dot{e} + K_p e = 0 \tag{27}$$

and

$$\begin{cases} K_v = 2\xi\omega, \\ K_p = \omega^2. \end{cases} \tag{28}$$

Consequently, the known performances of the computed torque control could thus be expected, with the prerequisite of a good dynamic modeling, a good dynamic identification and a good algorithm for the remaining numerical transformation.

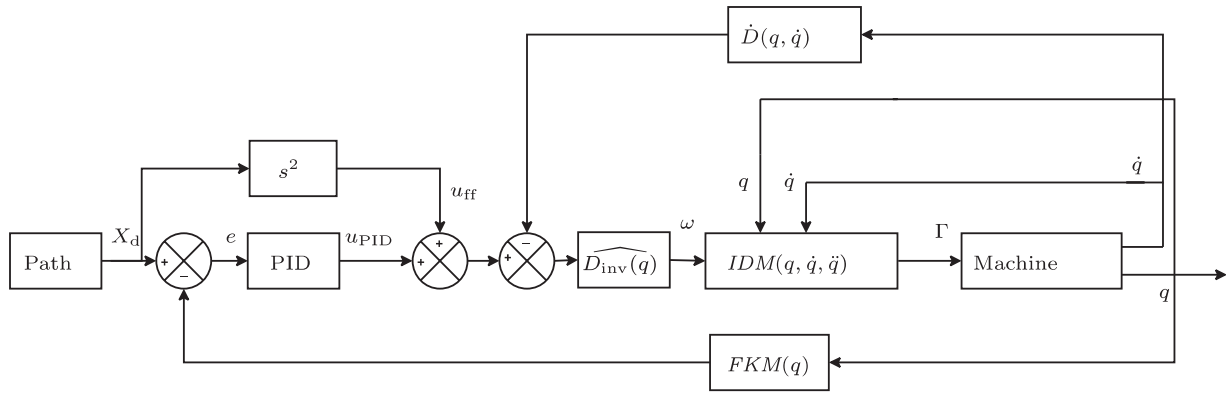


Fig. 9. Cartesian space computed torque control for serial kinematic machines.

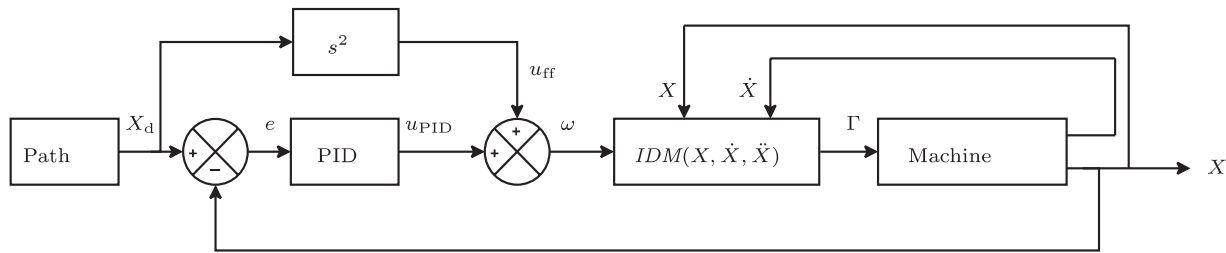


Fig. 10. Cartesian space computed torque control for parallel kinematic machines.

### 3.3. Discussion

#### 3.3.1. Joint Space or Cartesian Space Control?

The Cartesian space control is particularly relevant for parallel kinematic machines. Theoretically, since the end-effector pose is the state of a parallel kinematic machine, the Cartesian space control ensures a state feedback control leading to a better accuracy than a joint space control which is not a state feedback control any more. Moreover, by using a Cartesian space inverse dynamic model in a Cartesian space computed torque control, a minimal use of numerical transformations is required leading to a fast, stable and accurate control, when a good model is used and a good dynamic identification is performed. Furthermore, some additional advantages can be noted when a fast and accurate end-effector pose measure is available (Assumption 1).

First of all, in a joint space control, the regulated error is the error between a transformed desired trajectory, thus biased by the modeling errors, and a measure not reflecting the real end-effector pose, insensitive to backlashes or deformation. On the other hand, in the Cartesian space control case, the regulated error is the error between the measured and desired end-effector trajectories. Consequently, a Cartesian space control ensures a direct task control and thus can be more accurate than a joint space control.

Second, since the inverse kinematic model is not used to compute the joint reference path (see Figures 5 and 10), the constraints on kinematic identification could be relaxed. Indeed, without any kinematic identification, the Cartesian control performs an accurate positioning of the end-effector, when a point-to-point task is desired, since the reference trajectory is not biased by the inverse kinematic model errors. Furthermore, as far as the trajectory tracking is concerned, the dynamic identification prevails against the kinematic version in the minimization of the dynamic modeling errors. In addition, a dynamic identification, which is linear, is easier to set up than a kinematic identification, which is non-linear.

Third, a Cartesian space control is more interesting in the neighborhood of singularities. Indeed, one joint variable configuration leads to several end-effector poses (Husty 1994). In the worst cases, a disturbance on joint trajectory can thus shift the end-effector pose without changing the joint configuration. This can happen, in particular, in the neighborhood of singularities (assembling mode changing trajectory (Chablat and Wenger 1998)) or in cups points (non-singular posture changing trajectory (Zein et al. 2006)). This change of the end-effector pose is not observed by a joint space control whereas a Cartesian space control is able to do so (see Figure 11). Consequently, the Cartesian space control tries to bring back the end-effector pose to its reference or fails when

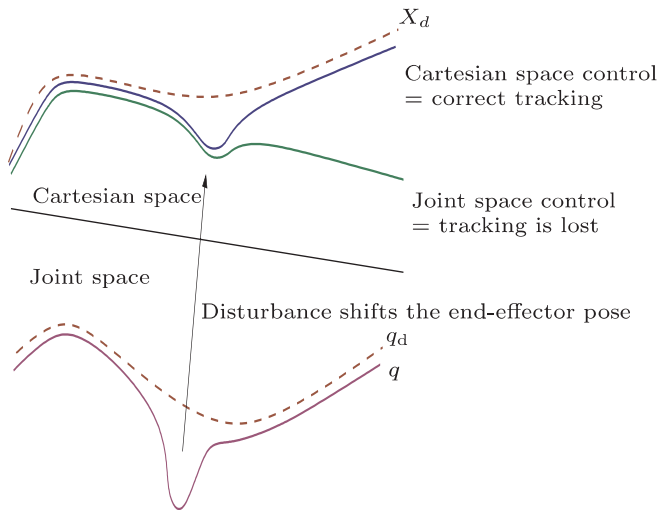


Fig. 11. Cartesian space ensures correct end-effector reference tracking in contrast to joint space control.

the singularity cannot be crossed again. In contrast, a converging joint space control cannot tell whether the Cartesian reference tracking fails or not. Consequently, a Cartesian space control can ensure a more reliable tracking than a joint space control.

Last but not least, even on a planned path taking into account kinematic and dynamic constraints, the joint position errors are independent of each other when using a joint space control. Therefore, the kinematic constraints cannot be ensured and two types of defect may appear: uncontrolled parasite end-effector moves or internal torques if these moves are impossible, thus degrading passive joints. In the same way as two-arm robot control (Dauchez et al. 1989), Cartesian space control can minimize, or cancel in the best cases, internal torques (Marquet et al. 2001). Indeed, the regulated errors, which are end-effector pose errors, are naturally compatible with the end-effector moves.

Consequently, the theoretical advantages of the Cartesian space control over the joint space one are now obvious. Therefore, the Cartesian space control seems perfectly relevant for the parallel kinematic machines and should always be used. However, the discussion made above assumes to have an available fast and accurate observation of the end-effector pose. This point remains the main issue making the Cartesian space control use occasional. Indeed, the measure of the end-effector pose is not an easy deal.

### 3.3.2. Comments on Assumption 1

In the literature, the observation is generally indirect: the end-effector pose is estimated throughout the forward kinematics problem solving (Beji et al. 1998; Yamane et al. 1998; Kock

and Shimacher 2000a; Marquet et al. 2001; Lee et al. 2003; Caccavale et al. 2003; Callegari et al. 2006). Thus, the numerical estimation issues, such as computation time, stability, reliability and accuracy, are retrieved here. In such a case, the property of a stable and accurate control is called into question and should be investigated. Nevertheless, adapted algorithms (Merlet 2004) or metrological redundancy (Baron and Angeles 2000; Marquet et al. 2002) can decrease the forward kinematics complexity and computation. Thus, it can improve the accuracy and stability of the control. However, the use of a kinematic model imposes heavy modeling and an accurate kinematic identification since the measure is biased by the kinematic errors.

Alternatively, instead of using a mechanical model, a direct measure can be used. To the best of the authors' knowledge, the means to measure the end-effector pose are few and far between. Laser trackers and computer vision are the main candidates. On the one hand, laser trackers allow for a very accurate and fast Cartesian position measure ( $20 \mu\text{m}$  and  $3 \text{ kHz}$ )<sup>1</sup>. Nevertheless, they are very expensive and hard to use. In addition, the orientation measure is not mastered. To the best of the authors' knowledge, they are only used for kinematic identification (Newman et al. 2000) and have never been used in the control loop.

On the other hand, computer vision is not as accurate and fast but is very easy to implement in a control scheme. It is a well-known solution for the kinematic control of a serial kinematic machine, namely visual servoing (Weiss et al. 1987; Espiau et al. 1992; Hutchinson et al. 1996). Recent works deal with visual servoing of a parallel kinematic machine and show good properties (Kino et al. 1999; Dallej et al. 2006). However, only this only concerns kinematic control. Ginhoux et al. (2004) proposed a fast visual servoing of a serial kinematic machine. However, the dynamics are compensated for with a robust controller and not with a computed torque control. To our mind, the application of such a control to parallel kinematic machines is not relevant according to what we stated above. A more relevant solution could be a visual computed torque control as initiated by Fakhry and Wilson (1996) for a serial kinematic machine. To the best of the authors' knowledge, there is no work on the fast visual servoing of parallel kinematic machine whereas good performances could be expected (Ait-Aider et al. 2006; Paccot et al. 2006).

To conclude, the Cartesian space control of parallel kinematic machines seems to be a relevant solution improving the accuracy, stability, speed, reliability and mechanical behavior. Let us now validate the theoretical discussion experimentally.

1. See <http://www.faro.com>.

**Table 1. Notation for the modeling of the Isoglide-4 T3R1.**

$X = [X_e \ Y_e \ Z_e \ \theta]^T$	Cartesian variables describing the end-effector pose $X$
$X_0, Y_0, Z_0, \delta_Z$	Constant parameters describing the reference position of each leg in the fixed basis
$q_{1i} = q_i, q_{2i}, q_{3i}$	Joint variables describing the leg $i$
$q_{jiki} = q_{ji} + q_{ki}$	Joint variables sum
$s_{ji} = \sin q_{ji}, c_{ji} = \cos q_{ji}$	Trigonometric operations on joint variables
$\Omega = [0 \ \dot{\theta} \ 0]^T$	Angular velocity of the end-effector
$L$	Length of the end-effector
$d_3, d_4$	Length of arm and forearm of a leg
$MR_1$	Mass of a leg
$MXR_2, MYG_2$	First moments of the arm of each leg around the $X$ - (grouped with other terms) and $Y$ -axes
$MXG_3, MYG_3$	First moments of the forearm of each leg around the $X$ - and $Y$ -axes
$ZZ_2, ZZR_3$	Inertia term of the forearm and the arm (grouped with other terms) of each leg around the $Z$ -axis
$Mcomp_3, Mcomp_4$	Equivalent mass of the forces applied by the compensator mounted on the vertical legs
$M_P$	Mass of the end-effector
$M_t = MR_1 + M_P$	Mass of the end-effector and a leg
$MS_P = [M_P X_P \ M_P Y_P \ M_P Z_P]$	Vector of the first moments of the end-effector around the fixed basis frame
$I_P$	Inertia matrix of the end-effector
$YY_P$	Inertia term of the end-effector around the $Z$ -axis
$g$	Acceleration of gravity

## 4. Modeling of the Test-bed

The notation used in this section is described in Table 1.

### 4.1. Presentation of the test-bed

The test-bed is the Isoglide-4 T3R1 (see Figure 12 and (Gogu 2004)). This parallel kinematic machine is fully isotropic with decoupled motion. It is a four-degrees-of-freedom machine with three translations and one rotation. This machine is composed of four identical legs. Each leg contains one actuated prismatic joint and two passive revolute joint, linked to the end-effector by one universal joint (see Figures 13 and 14). The actuation is performed with linear motors.

This machine is designed for high-speed machining. Hence, the structure weight is important to meet the stiffness requirements: 31 kg for each leg and 14 kg for the end-effector. Therefore, the leg dynamics have a great influence and thus cannot be neglected, in contrast to common light parallel kinematic machines for pick-and-place. Consequently, a complete dynamic modeling and a performant dynamic control is required to ensure the high accuracy required in machining. This test-bed is thus relevant for validating the assumption made on the weakness of single-axis linear control.

The main advantage of the Isoglide-4 T3R1, as far as control is concerned, is to have a closed-form expression of the forward kinematic and instantaneous kinematic models:

$$\begin{cases} X_e = q_1 - X_0, \\ Y_e = q_2 - Y_0, \\ Z_e = q_3 - Z_0, \\ \sin \theta = \frac{q_4 - q_3 + \delta Z}{L}. \end{cases} \quad (29)$$

and

$$D(X) = \begin{pmatrix} 1 & 0 & 0 & 0 \\ 0 & 1 & 0 & 0 \\ 0 & 0 & 1 & 0 \\ 0 & 0 & -\frac{1}{L \cos \theta} & \frac{1}{L \cos \theta} \end{pmatrix}. \quad (30)$$

Therefore, the simple and closed-form expression of the forward kinematics are interesting for validating the proposed

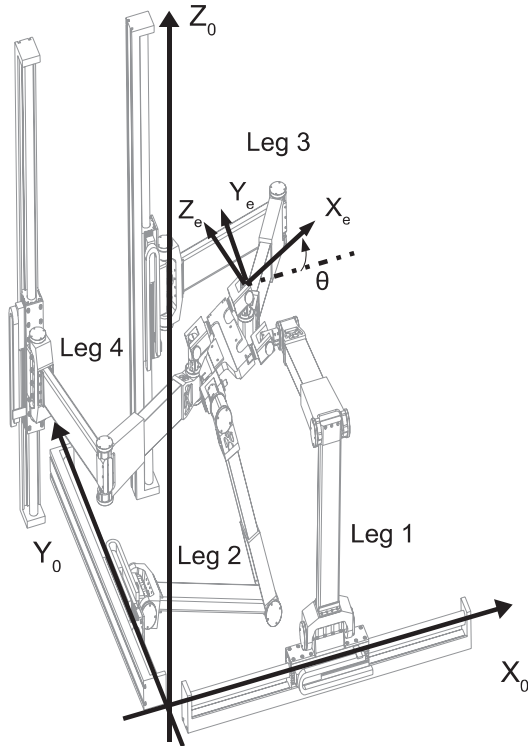


Fig. 12. Global view of the Isoglide-4 T3R1.

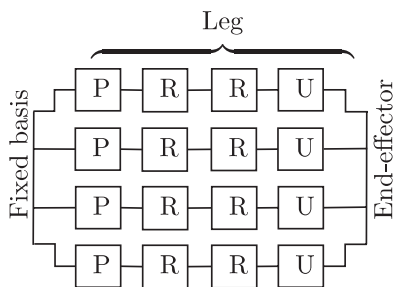


Fig. 13. Kinematic scheme of the Isoglide-4 T3R1.

Cartesian space control schemes. Indeed, it removes issues from the numerical estimation and the lack of fast and accurate end-effector pose measure. Therefore, a fairer comparison between forward kinematic model based control and exteroceptive measure based control could be achieved. Actually, the influence of the numerical estimations issues on control behavior, which are hard to quantify, are removed. The comparison can only be achieved in term of sensor and identification accuracy with regards to the control accuracy.

4.2. Dynamic Modeling

Achieving a performant computed torque control requires a Cartesian space dynamic modeling method with an easy

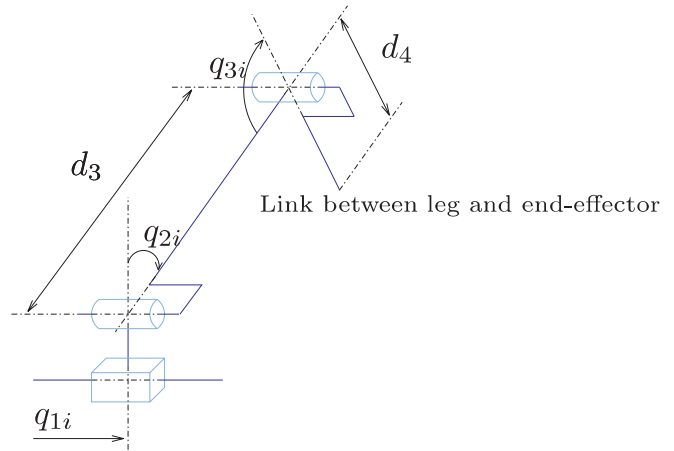


Fig. 14. Detail of one leg.

implementation, a low computation cost and minimal simplifications. In this way, the method of Khalil and Ibrahim (2004) is preferred to other known methods (Dasgupta and Choudhury 1999; Tsai 2000; Callegari et al. 2006). Indeed, it is based on the Newton–Euler algorithm, known to be relevant in a control context. Moreover, the application of the method is easy due a very simple formulation.

According to Khalil, the inverse dynamic model can be simply expressed as (Khalil and Ibrahim 2004):

$$\Gamma = \widehat{D}^T \left( \mathbb{F}_p + \sum_{i=1}^n J_{pi}^T D_i^T (\mathbb{H}_i + \mathbb{G}_i) \right) + \Gamma_f, \quad (31)$$

where:

- $\mathbb{F}_p$  are the dynamics of the end-effector;
- $n$  is the number of legs;
- $D_i$  is the inverse instantaneous kinematic matrix of leg  $i$ ;
- $J_{pi}$  is a Jacobian matrix linking the Cartesian coordinates of the end of the leg  $i$  to the Cartesian coordinates of the end-effector;
- $\mathbb{H}_i$  are the dynamics of the leg  $i$ ;
- $\mathbb{G}_i$  is the gravity vector of the leg  $i$ .

This modeling method is thus achieved through a complete modeling of each leg and a determination of the end-effector dynamics.

4.2.1. Modeling of Each Leg

A leg can be seen as a stand-alone 3-PRR serial kinematic machine. The modeling of such a serial kinematic machine is well

known. Consequently, we only give the obtained models without details on the method. The kinematics are determined with Khalil–Kleinfinger notation, the dynamics with the Newton–Euler algorithm and the notation of Khalil and Dombre (2002).

The inverse instantaneous kinematic matrix of leg 1 can be expressed as

$$D_1 = \begin{pmatrix} 1 & 0 & 0 \\ 0 & \frac{s_{2131}}{d_3 s_{31}} & \frac{c_{2131}}{d_3 s_{31}} \\ 0 & \frac{d_4 s_{2131} + d_3 s_{21}}{d_4 d_3 s_{31}} & \frac{d_4 s_{2131} + d_3 s_{21}}{d_4 d_3 s_{31}} \end{pmatrix}. \quad (32)$$

Each term of the inverse dynamics of the first leg,  $\mathbb{H}_1 = [H_{11} \ H_{12} \ H_{13}]^T$  are detailed below:

$$H_{11} = MR_1 \dot{q}_{11}, \quad (33)$$

$$\begin{aligned} H_{12} = & (ZZR_2 + 2d_3 MXG_3 c_{31} - 2d_3 MYG_3 s_{31}) \ddot{q}_{21} \\ & + (ZZ_3 + d_3 MXG_3 c_{31} - d_3 MYG_3 s_{31}) \ddot{q}_{31} \\ & + (d_3 MXG_3 s_{31} + d_3 MYG_3 c_{31}) \dot{q}_{21}^2 \\ & - (d_3 MXG_3 s_{31} + d_3 MYG_3 c_{31}) \dot{q}_{2131}^2, \end{aligned} \quad (34)$$

$$\begin{aligned} H_{13} = & (ZZ_3 + d_3 MXG_3 c_{31} - d_3 MYG_3 s_{31}) \ddot{q}_{21} \\ & + (ZZ_3) \ddot{q}_{31} \\ & + (d_3 MXG_3 s_{31} + d_3 MYG_3 c_{31}) \dot{q}_{21}^2. \end{aligned} \quad (35)$$

The passive joint variables are expressed as function of the end-effector pose with simple trigonometric relations. Other legs have similar models. The change comes from the position of the legs in the Cartesian space, modifying the gravity terms and Jacobian matrix organization. The gravity vectors,  $\mathbb{G}_i$ , for each leg are detailed below:

$$\mathbb{G}_1 = \begin{bmatrix} 0 \\ (MXR_2 s_{21} + MYG_2 c_{21} + MXG_3 s_{2131} + MYG_3 c_{2131})g \\ (MXG_3 s_{2131} + MYG_3 c_{2131})g \end{bmatrix} \quad (36)$$

$$\mathbb{G}_2 = \begin{bmatrix} 0 \\ (MXR_2 c_{22} + MYG_2 s_{22} + MXG_3 c_{2232} + MYG_3 s_{2232})g \\ (MXG_3 c_{2232} + MYG_3 s_{2232})g \end{bmatrix} \quad (37)$$

$$\mathbb{G}_3 = \begin{bmatrix} (-MR_1 + Mcomp_3)g \\ 0 \\ 0 \end{bmatrix} \quad (38)$$

$$\mathbb{G}_4 = \begin{bmatrix} (-MR_1 + Mcomp_4)g \\ 0 \\ 0 \end{bmatrix} \quad (39)$$

Two gravity compensators are used for the vertical legs, namely the third and fourth, explaining the presence of terms

$Mcomp_3$  and  $Mcomp_4$ . Their influence is approximated as constant.

The Jacobian matrices  $J_{pi}$  have a very simple expression. Indeed, the end of each leg is defined by its Cartesian position. The end-effector is defined by four Cartesian variables  $[X_e \ Y_e \ Z_e \ \theta]^T$ . For the first and third legs, there is only an offset between the Cartesian position of the legs and the end-effector and the orientation  $\theta$  has no influence. For the two other legs, the orientation  $\theta$  has an influence which is easily determined with trigonometric relations. Consequently, the matrices have the following expressions:

$$J_{p1} = J_{p3} = \begin{bmatrix} 1 & 0 & 0 & 0 \\ 0 & 1 & 0 & 0 \\ 0 & 0 & 1 & 0 \end{bmatrix} \quad (40)$$

$$J_{p2} = J_{p4} = \begin{bmatrix} 1 & 0 & 0 & Ls_\theta \\ 0 & 1 & 0 & 0 \\ 0 & 0 & 1 & Lc_\theta \end{bmatrix}. \quad (41)$$

#### 4.2.2. Dynamics of the End-effector

The dynamics of the end-effector are determined with the Newton–Euler equation (Khalil and Dombre 2002; Khalil and Ibrahim 2004):

$$\mathbb{F}_p = \gamma_p \ddot{X} + \begin{bmatrix} \Omega \times (\Omega \times MS_p) \\ \Omega \times \Omega \end{bmatrix} - \begin{bmatrix} M_p I_3 \\ \widehat{MS_p} \end{bmatrix} g, \quad (42)$$

where  $\gamma_p$  is the inertia tensor of the end-effector expressed as

$$\gamma_p = \begin{pmatrix} M_p I_3 & -S(MS_p) \\ S(MS_p) & I_p \end{pmatrix} \quad (43)$$

Only the terms along the end-effector degrees of freedom are retained which yields the final expression of the end-effector dynamics as shown in Table 2.

#### 4.2.3. Inverse Dynamic Model of the Isoglide-4 T3R1

The inverse dynamic model is obtained using (31). For the sake of being concise, the global expression is not mentioned here. Nevertheless, the model obtained has a closed-form expression allowing for an interpretation of each term. The main term is the inertia of the legs and the end-effector in translation, this term thus has a great influence on the tracking performances. Then the other main terms concern the coupling between legs

**Table 2. The final expression of the end-effector dynamics.**

$$\mathbb{F}_P = \begin{pmatrix} M_P \ddot{X}_e + (M_P X_{Ps\theta} + M_P Z_{Pc\theta}) \ddot{\theta} + (-M_P X_{Pc\theta} + M_P Z_{Ps\theta}) \dot{\theta}^2 \\ M_P \ddot{Y}_e \\ M_P (\ddot{Z}_e - g) + (-M_P X_{Pc\theta} + M_P Z_{Ps\theta}) \ddot{\theta} - (M_P X_{Ps\theta} + M_P Z_{Pc\theta}) \dot{\theta}^2 \\ Y Y_P \ddot{\theta} + (M_P X_{Ps\theta} + M_P Z_{Pc\theta}) \ddot{X}_e + (-M_P X_{Pc\theta} + M_P Z_{Ps\theta}) (\ddot{Z}_e - g) \end{pmatrix}$$

due to the heavy inertia. Even if a kinematic decoupling is ensured, the dynamic coupling remains present and cannot be compensated for with a linear control. The last term concerns the rotation inertia of the end-effector: this term is not preponderant and can be neglected if necessary.

A simple friction forces model is implemented to compensate for the latter and improve accuracy:

$$\Gamma_f = (F_v \dot{q} + F_s) \text{sign}(\dot{q}). \tag{44}$$

## 5. Results

### 5.1. Simulation

First, the improvement of the joint space computed torque control (Figure 5) over the single-axis (Figure 2) control is shown. A comparison is achieved in terms of the straightness error and tracking error on a relevant trajectory. Second, a comparison between computed torque control in the joint space and in the Cartesian space (Figures 5 and 10) is performed. The Cartesian space computed torque control is performed with the forward kinematics and with a direct measure to emphasize the improvement when using the direct measure rather than the forward kinematics.

The machine behavior is simulated with the forward dynamic model obtained by inverting (31) which allows the end-effector acceleration to be computed (see Figure 15). Realistic noises and errors are used, such as a 10% error on dynamic parameters, 50 μm accuracy for geometric parameters (required manufacturing and assembly tolerance for the Isoglide-4 T3R1). Let us stress that neither deformations nor assembly errors (such as a non-perpendicular axis) are simulated. A 1 μm accuracy is fixed for the joint sensors, and a 20 μm and 10<sup>-4</sup> rad accuracy for the direct measure (laser tracker performance). The tuning is done with ω = 5 Hz and the control and sensors have a 1 kHz sampling rate.

The reference trajectory, Figure 16, is composed of one translation along the X-axis, one translation along X-, Y- and Z-axes and one translation along the three axes with a rotation. The first part of the trajectory allows for pointing out the ability of the control strategy to compensate for the dynamic coupling between legs. The second part allows for comparing the compensation of the inertia forces. The last part allows for a comparison of joint space control and Cartesian space control performed with forward kinematics and direct end-effector

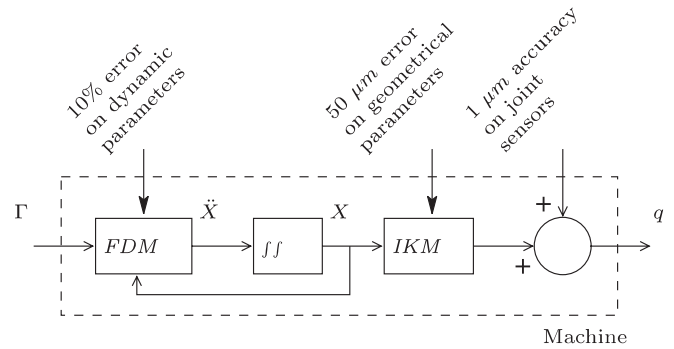


Fig. 15. Dynamic model of the machine used in simulation.

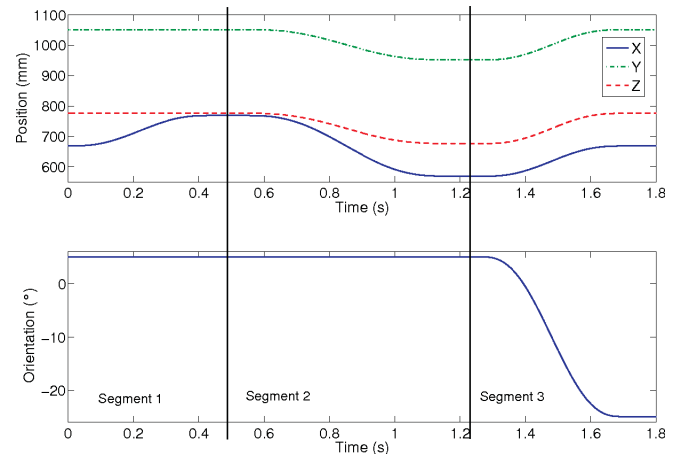


Fig. 16. Reference trajectory in Cartesian space.

pose measure. Indeed, there is only a difference, between forward and inverse kinematics, on the rotation since the Isoglide-4 T3R1 has decoupled translations (see (29)).

A fifth-degree polynomial point-to-point interpolation is used to have a smooth trajectory. The maximal acceleration is fixed to 3 m s<sup>-2</sup> to simulate a machining operation. This low speed is far from the high-speed pick-and-place situation.

#### 5.1.1. Joint Space Computed Torque Control versus Single-axis Control

Figure 17 shows the trajectory in the XY plane performed by the two control strategies, single-axis control and the com-

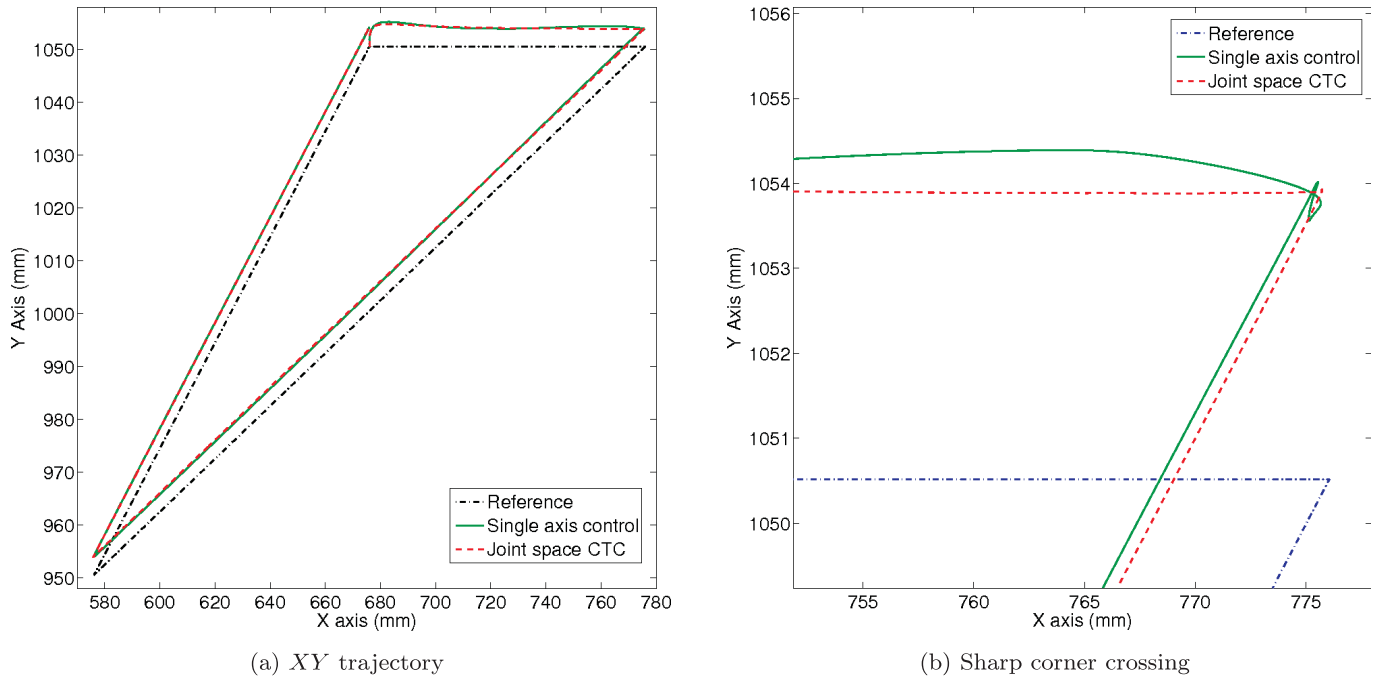


Fig. 17. Comparison, in the  $XY$  plane, between single-axis linear control and the joint space computed torque control.

**Table 3. Straightness error on each segment measured in simulation.**

	Single-axis	Joint space computed torque control
First segment	0.759 mm	0.026 mm
Second segment	1.900 mm	0.089 mm
Third segment	3.758 mm	0.180 mm

puted torque control in the joint space, and the reference. In Figure 17(a), the two control strategies are biased with regards to the reference trajectory. Figure 17(b) shows the details of a sharp corner crossing, with zero speed, and reveals a difference between single-axis and computed torque control. Indeed, the trajectory followed with the single-axis control is not completely straight and presents some oscillations in the corner, in contrast to the joint space computed torque control. This is numerically verified in Table 3. The computed torque control allows for straightness errors about 20 times less important than single-axis control does. Figure 18 shows the tracking error on  $X$ -axis for the same two control strategies. The single-axis control presents important tracking errors with a maximum along the four axes displacement (2.5 mm peak to peak). On the opposite, the computed torque control allows for small tracking errors. These errors are distributed around the constant bias, 318  $\mu\text{m}$ , between the performed trajectory and the reference trajectory.

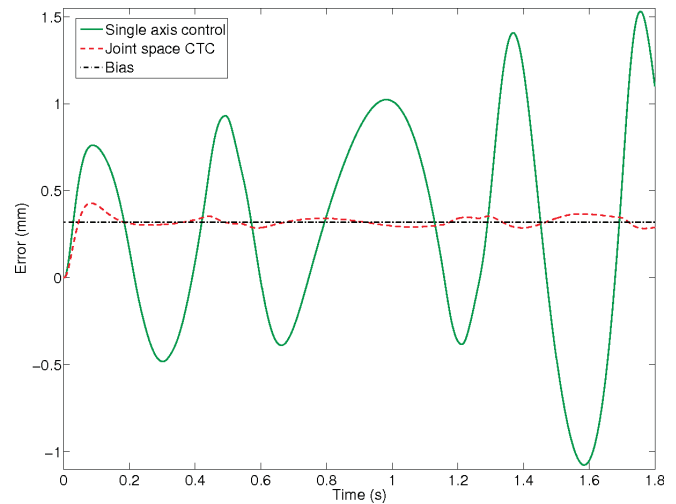


Fig. 18. Tracking error on the  $X$ -axis for the single-axis linear control and joint space computed torque control, and bias between the reference and performed trajectory.

Thus, using a computed torque control instead of simple control improves the dynamic accuracy of the machine. Indeed, the high dynamic coupling between legs, due to important masses, is clearly not negligible, even at machining speed often considered as quasi-static. Therefore, the complete machine dynamics should be taken into account in the control loop. Moreover, the strong influence of the kinematic iden-

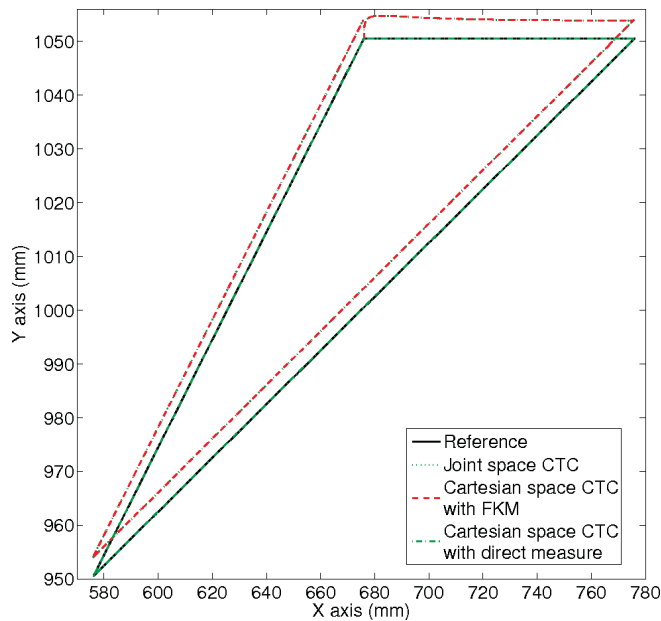


Fig. 19. A comparison, in the XY plane, between joint and Cartesian space computed torque control, with forward kinematics and direct end-effector pose measure.

tification is retrieved here. Actually, there is a bias between the Cartesian reference and the joint reference, due to remaining kinematic errors. In the Isoglide-4 T3R1 case, this bias is constant and can be seen as an adjustable offset. However, in more complex cases, this bias is not constant along the workspace and thus cannot be compensated for without a more accurate kinematic identification asking for a more accurate measure and heavier computation.

### 5.1.2. Joint Space Computed Torque Control versus Cartesian Space Computed Torque Control

Figure 19 show the performed trajectory in the XY plane by the joint space computed torque control, the Cartesian space computed torque control with forward kinematics and the Cartesian space computed torque control with direct end-effector pose measure. The first two control strategies have exactly the same behavior and bias with regards to the reference trajectory. On the other hand, the trajectory performed by the computed torque control with direct end-effector pose measure does not present a bias and is mixed with the reference trajectory. Figure 20 shows the orientation tracking error for the computed torque control in the joint and the Cartesian space. Joint space and Cartesian space, with forwards kinematics, computed torque control have exactly the same behavior. The computed torque control with direct end-effector pose measure allows for better accuracy than the two other

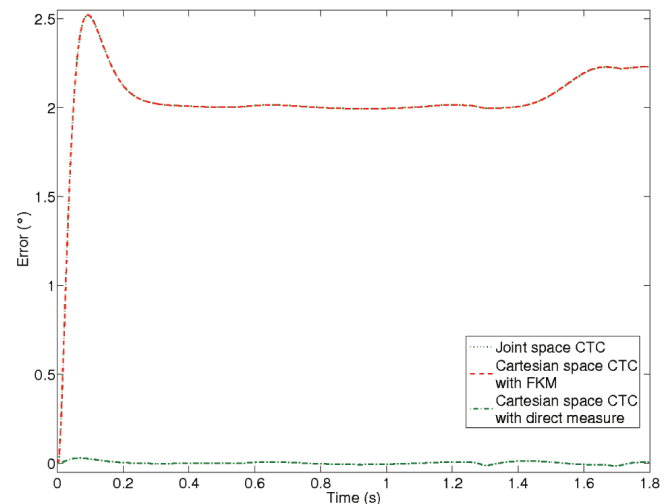


Fig. 20. A comparison of the orientation error tracking between joint space and Cartesian space control, with forward kinematics and a direct measure of the end-effector pose.

control strategies, since there is no bias and there are better tracking performances during the rotation at the end of the trajectory, between 1.3 and 1.8 seconds. The tracking performances are numerically summarized in Tables 4 and 5. The joint space computed torque and the Cartesian space computed torque control with forward kinematics have strictly the same performances. On the opposite, the use of a direct end-effector measure allows for better mean errors (13 versus 322  $\mu\text{m}$ ) and similar standard deviation for the X-axis and straightness errors. Concerning the orientation, the direct measure allows for a tracking error 30 times less important than the forward kinematics.

The use of the Cartesian space control with a direct measure of the end-effector pose instead of a joint space control does improve static and dynamic accuracy, whereas a forward kinematics based control only allows for good dynamic performances but reduced geometric accuracy. Indeed, the use of a direct measure allows us to compensate for the kinematic errors without concerning ourselves with extremely accurate kinematic identification. The performed trajectory is not shifted with respect to the reference trajectory. Furthermore, it needs to be underlined that even though the direct measure is less accurate than the joint sensors, using it for control ensures equivalent translation tracking performance and better orientation performance. By improving the measure accuracy, we can improve the performance of the control law. In this case, the sensor accuracy thus has more influence on the control accuracy than the modeling errors. Finally, the numerical results show that a 100  $\mu\text{m}$  accuracy, which is the minimum required in machining, can be achieved with the computed torque control without particular care. Nevertheless, this can be still im-

**Table 4. Straightness error on each segment measured in simulation.**

	Joint space computed torque control	Computed torque control with forward kinematic model	Computed torque control with direct measure
First segment	0.026 mm	0.026 mm	0.040 mm
Second segment	0.089 mm	0.089 mm	0.083 mm
Third segment	0.180 mm	0.180 mm	0.147 mm

**Table 5. Tracking errors along the trajectory.**

Control	Mean of tracking error on $X$	Standard deviation of tracking error on $X$	Mean of tracking error on $\theta$	Standard deviation of tracking error on $\theta$
Joint space computed torque control	0.322 mm	0.024 mm	2°	0.079°
Computed torque control with forward kinematic model	0.322 mm	0.024 mm	2°	0.079°
Computed torque control with direct measure	0.013 mm	0.026 mm	0°	0.006°

proved with less error on parameters (in other words a better identification), a more elaborated gain tuning and a more accurate sensor.

## 5.2. Experiments

### 5.2.1. Dynamic Identification

In order to fit the inverse dynamic model to the real dynamics of the machine and ensure the best performances for computed torque control, dynamic identification was realized (see Table 6). The method used here was proposed by Guegan et al. (2003). The chosen exciting trajectory is composed of axis-by-axis displacements with acceleration ranging from 0.5 to 3 m s<sup>-2</sup>. A simulation on different trajectories (circles, axis-by-axis displacements, coupled axis displacement and random trajectory) shows that the axis-by-axis displacements obtained the best condition number. Indeed, it allows both free and constrained moves on each axis. The parameters concerning the dynamic coupling are thus determined with the torques recorded during free moves. Those concerning the inertia terms are determined during constrained moves.

Results lead to an observation matrix condition number of 355.56 which is relatively good. Inertia parameters ( $MXR_3$ ,  $ZZR_3$ ,  $ZZR_2$ ,  $M_i$ ,  $M_{R1}$ ) are identified with a standard deviation from 0.40% to 1.29%, friction terms ( $Fs_i$  and  $Fv_i$ ) from 1.07% to 6.34%. Let us remark that some parameters describing the end-effector cannot be identified because the end-effector is lighter than the legs, thus having little influence on the dynamics. Anyhow, the good results of the identification process allow for the fulfillment of the small modeling errors condition, necessary to ensure a stable and accurate computed torque control.

### 5.2.2. Experiments

The simulation showed that a Cartesian space computed torque control with forward kinematics and a joint space computed torque control have the same behavior. The expected improvements could only be established with a control using a direct measure of the end-effector pose. At the moment, the computer vision is not accurate and fast enough to set up relevant experiments and a laser tracker is too expensive. Consequently, we can only propose an experimental comparison between single-axis control and computed torque control in the Cartesian space with the forward kinematics. To achieve this comparison, the end-effector trajectory is measured with a 512 × 512 camera as an exteroceptive measure running at 250 Hz. This provides us with a measure of the real end-effector trajectory instead of a model biased estimation. A comparison between the camera and a laser interferometer is performed (see Figure 21). Figure 22 shows that the camera has an average accuracy of 26 μm compared with the interferometer measure thus validating further results.

Both control schemes have the same gain tuning with the same cut-off frequency ( $\omega_c$ ) of 5 Hz. Nevertheless, the derivative gain in the single-axis controller cannot be set at its theoretical value because the linear actuators we use do not cope with noise, even if filtered. The reference trajectory is a simple 100 mm<sup>2</sup> square in the  $XY$  frame. A fifth-degree path generation with a 3 m s<sup>-2</sup> maximal acceleration is used. The trajectory is executed in a segment-by-segment manner.

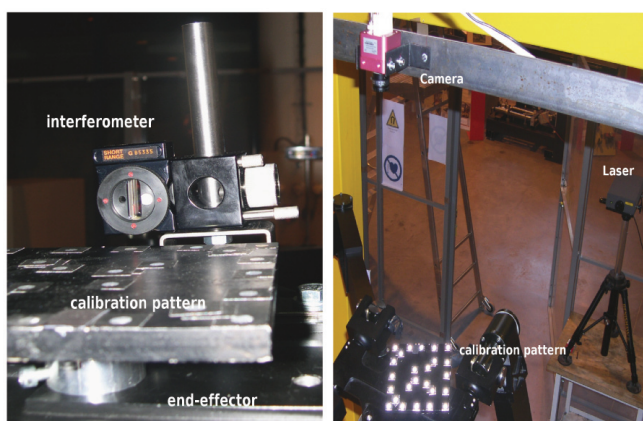
Figure 23 shows the performed trajectory in the  $XY$  plane for the two control strategies, single-axis and computed torque control, compared with the reference trajectory. Let us stress that Figure 23 only represents the relative displacements. Thus,

**Table 6. Dynamic identification results.**

Parameter	CAD values	Identified values	Units	$\sigma$ (%)
$MXR_3$	3.235	5.054	$kg.m$	0.42
$MYG_3$	0	0	$kg.m$	
$MXR_2$	7.971	0	$kg.m$	
$MYG_2$	0	0	$kg.m$	
$ZZ_3$	1.787	2.443	$kg.m^2$	1.29
$ZZR_2$	6.429	8.420	$kg.m^2$	0.54
$M_t$	45.011	39.513	$kg$	0.62
$M_{R1}$	31.4380	39.999	$kg$	0.40
$M_P X_P$	2.059	0	$kg.m$	
$M_P Z_P$	0	0	$kg.m$	
$YY_P$	0.411	0	$kg.m$	
$M_{comp_3}$	45.011	49.180	$kg$	0.50
$M_{comp_4}$	31.4380	41.005	$kg$	0.39
$F_{s1}$		10.907	$N$	2.76
$F_{s2}$		25.558	$N$	1.25
$F_{s3}$		21.044	$N$	1.71
$F_{s4}$		28.980	$N$	1.07
$F_{v1}$		36.108	$N.s.m^{-1}$	3.81
$F_{v2}$		89.419	$N.s.m^{-1}$	2.45
$F_{v3}$		35.211	$N.s.m^{-1}$	6.34
$F_{v4}$		64.793	$N.s.m^{-1}$	3.10

Observation matrix condition number: 355.56

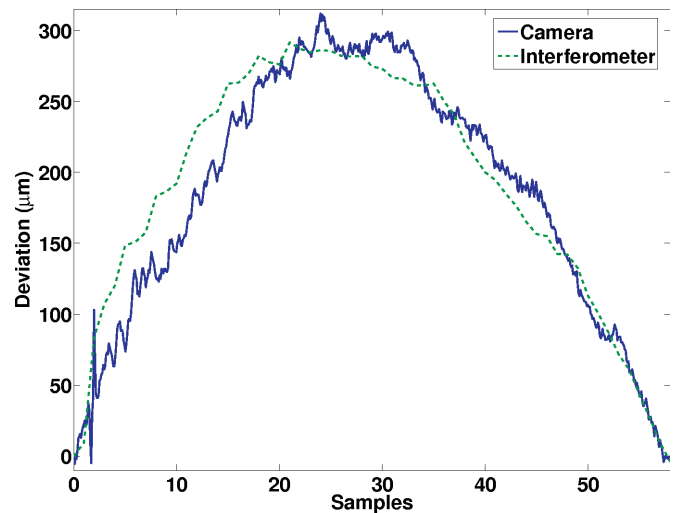
Number of samples: 65404



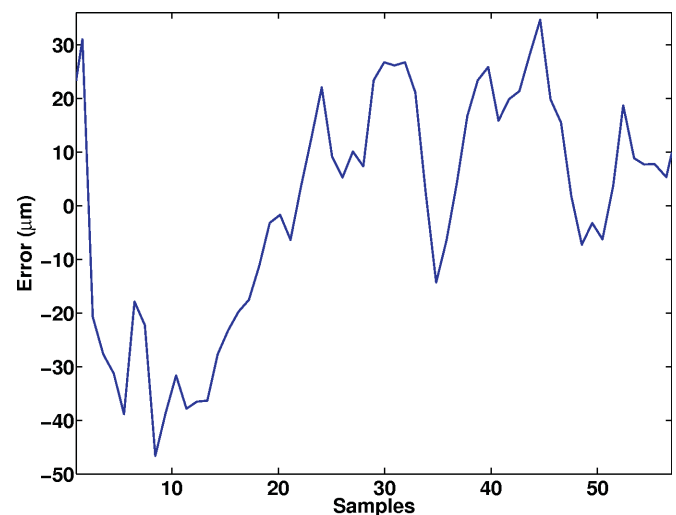
(a) Calibration pattern and interferometer mounted on the end-effector

(b) Camera and laser

Fig. 21. Straightness measure with a high-speed camera and a laser interferometer.



(a) Deviation on the Y-axis



(b) Error between the laser interferometer and camera measures

Fig. 22. Comparison between the laser interferometer and the camera.

the bias due to the geometrical errors is not measured. The computed torque control achieves an accurate tracking while the single axis cannot. Indeed, the computed torque control performs straight displacements whereas the single-axis control presents some oscillations around the reference. Numerically, the straightness error are divided by 7 for the X-axis displacement and 10 for the Y-axis displacement (see Table 7). Figure 24 shows the time evolution of the end-effector position along the X-axis for the reference trajectory, the single axis control and the computed torque control. It should be noted

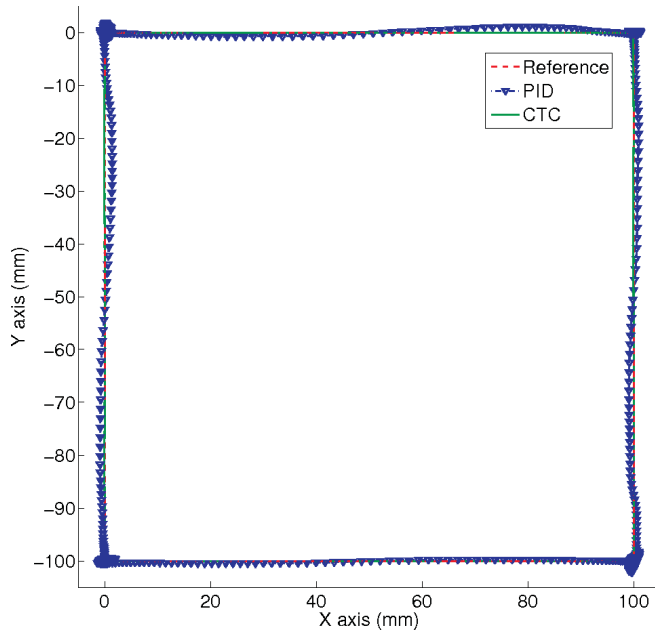


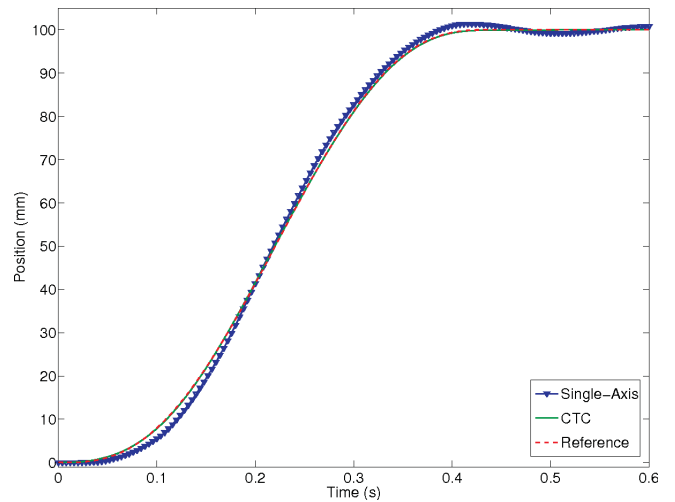
Fig. 23. Comparison between the single-axis and computed torque controller measured with a high-speed camera on a 100 mm XY square.

**Table 7. Measured straightness error on the square segments with a high-speed camera.**

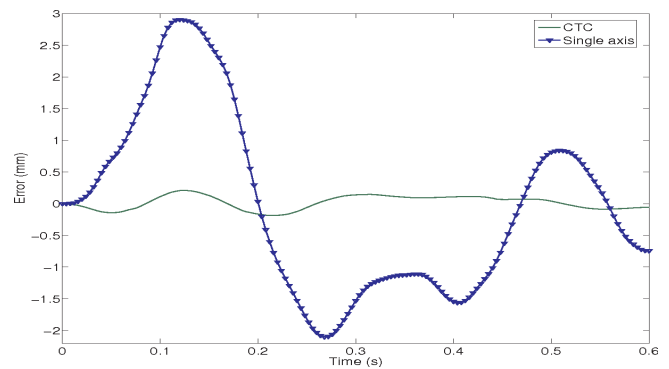
	PID	Computed torque control
Left edge	0.733 mm	0.154 mm
Right edge	2.255 mm	0.330 mm
Bottom edge	3.318 mm	0.443 mm
Top edge	3.143 mm	0.293 mm

that the computed torque control presents good tracking performance whereas the single-axis control presents important tracking errors and overshoot.

Thus, these experiments validate the simulation results above. In other words, using computed torque control instead of a linear single-axis control improves tracking. It should be noted that the obtained results are worse than expected. Indeed, simulations do not take into account assembly defects, making the difference between the simulated model and the control model smaller than the difference between the real machine and the control model. The assembly defects are treated in the kinematic models (Rizk et al. 2006) and should be extended to dynamics. In addition, a more accurate identification with exteroceptive measure, such as computer vision (Renaud et al. 2006), could be used to improve control accuracy.



(a) End-effector pose along the X-axis



(b) Tracking error along the X-axis

Fig. 24. End-effector pose along the X-axis measured with a high-speed camera on a 100 mm<sup>2</sup> square.

## 6. Conclusion

In this article, our aim was to show that control of a parallel kinematic machine should be rethought. To our mind, a computed torque control in the Cartesian space, with an exteroceptive end-effector pose measure and a Cartesian space dynamic model, is the relevant solution to ensure the best performance and use of the machine capabilities.

Indeed, the inherent complexity of the closed mechanical structure leads to highly non-linear dynamics with dynamic leg coupling. Therefore, a single-axis control cannot ensure correct performance while using the whole workspace and the machine maximal speed capabilities. In this way, the computed torque control is known to be a relevant solution for serial kinematic machines. However, the computed torque control is often forsaken by the parallel kinematic machine community

since it often requires robust control. Nevertheless, these control schemes of serial robotics are classically performed in the joint space and thus should not be reused directly for parallel kinematic machines.

Actually, since a parallel kinematics machine is defined by its end-effector configuration, using a Cartesian space control is more relevant than using the classical joint space control. In addition, when it is performed with an exteroceptive end-effector pose measure, the modeling errors sources are minimized leading to a more stable control than the joint space control, making the robust control useless or, at least, used only for unknown disturbances rejection. Furthermore, we showed that a Cartesian space control allows for a better mechanical structure handling than the joint space control.

Simulations were performed to validate the above discussion and some of them were validated experimentally. Nevertheless, further experiments should be performed to validate the improvement of the use of an exteroceptive measure of the end-effector, such as computer vision or laser tracker. These experiments should be preceded by a more performant identification. The test-bed is very particular, therefore experiments on other structures, such as the Gough–Stewart platform, should be done to validate the genericity of the approach and validate the internal torque minimization and the behavior in the neighborhood of singularities. Last but not least, a theoretical demonstration of the control accuracy, stability and robustness in regards with measure and modeling errors could be performed as initiated by Paccot et al. (2007).

## References

- Abdellatif, H. and Heiman, B. (2005). Adapted time-optimal trajectory planning for parallel manipulators with full dynamic modeling. *Proceedings of the International Conference on Intelligent Robots and Systems (IROS'05)*, Edmonton, Canada, 2005, pp. 411–416.
- Ait-Aider, O., Andreff, N., Lavest, J. and Martinet, P. (2006). Simultaneous object pose and velocity computation using a single view from a rolling shutter camera. *Proceedings of the European Conference on Computer Vision (ECCV'06)*, Graz, Austria, 2006, pp. 56–68.
- Ait Aider, O., Paccot, F., Andreff, N. and Martinet, P. (2006). A novel approach to vision-based computed torque control of parallel robots. *Proceedings of the 12th IEEE International Conference on Methods and Models in Automation and Robotics MMAR'06*, Miedzydroje, Poland, 2006.
- Baron, L. and Angeles, J. (2000). The direct kinematics of parallel manipulators under joint-sensor redundancy. *IEEE Transactions on Robotics and Automation*, **16**(1): 1–8.
- Barrette, G. and Gosselin, C. (2005). Determination of the dynamic workspace of cable-driven planar parallel mechanisms. *ASME Journal of Mechanical Design*, **127**(2): 242–248.
- Beji, L., Abichou, A. and Pascal, M. (1998). Tracking control of a parallel robot in the task space. *Proceedings of the International Conference on Robotics and Automation (ICRA'98)*, Leuven, Belgium, pp. 2309–2314.
- Besnard, S. and Khalil, W. (1999). Calibration of parallel robots using two inclinometers. *Proceedings of the IEEE International Conference on Robotics and Automation (ICRA'99)*, Detroit, MI, pp. 1758–1763.
- Brecher, C., Ostermann, T. and Friedich, D. (2006a). Control concept for PKM considering the mechanical coupling between actuators. *Proceedings of the Chemnitz Parallel Kinematics Seminar* Chemnitz, Germany, 2006, 413–427.
- Brecher, C., Weck, M. and Yamasaki, T. (2006b). Controller-integrated predictive oscillation compensation for machine tools with parallel kinematics. *Machine Tools and Manufacture*, **46**: 142–150.
- Caccavale, F., Siciliano, B. and Villani, L. (2003). The Tricept robot: dynamics and impedance control. *IEEE Transactions on Mechatronics*, **8**: 263–268.
- Callegari, M., Palpacelli, M. and Principi, M. (2006). Dynamics modelling and control of the 3-RCC translational platform. *Mechatronics*, **16**: 589–605.
- Chablat, D. and Wenger, P. (1998). Working modes and aspects in fully parallel manipulators. *Proceedings of the IEEE International Conference on Robotics and Automation (ICRA'98)*, Leuven, Belgium, pp. 1964–1969.
- Chanal, H., Duc, E. and Ray, P. (2006a). A study of the impact of machine tool structure on machining processes. *International Journal of Machine Tools and Manufacture*, **46**: 98–106.
- Chanal, H., Duc, E., Ray, P. and Hascoët, J. (2006b). A new approach for the geometrical calibration of parallel kinematics machines tools based on the machining of a dedicated part. *International Journal of Machine Tools and Manufacture*, **47**(7–8): 1151–1163.
- Company, O. and Pierrot, F. (2002). Modelling and design issues of a 3-axis parallel machine-tool. *Mechanism and Machine Theory*, **37**(11): 1325–1345.
- Dallej, T., Andreff, N., Mezouar, Y. and Martinet, P. (2006). 3D pose visual servoing relieves parallel robot control from joint sensing. *Proceedings of the International Conference on Intelligent Robots and Systems (IROS'06)*, Beijing, China, pp. 4291–4296.
- Daney, D. (1999). Self calibration of Gough platform using leg mobility constraints. *Proceedings of the World congress on the theory of machine and mechanisms (IFTOMM)*, Oulu, Finland, pp. 104–109.
- Dasgupta, B. and Choudhury, P. (1999). A general strategy based on the Newton–Euler approach for the dynamic formulation of parallels manipulators. *Mechanism and Machine Theory*, **34**: 801–824.
- Dauchez, P., Delebarre, X. and Jourdan, R. (1989). Hybrid control of a two-arm robot handling firmly a single rigid object. *Proceedings of the 2nd International Workshop*

- on *Sensorial Integration for Industrial Robots (SIFIR'89)*, Zaragoza, Spain, pp. 67–62.
- Denkena, B. and Holz, C. (2006). Advanced position and force control concepts for the linear direct driven hexapod PaLiDA. *Proceedings of the Chemnitz Parallel Kinematics Seminar*, Chemnitz, Germany, pp. 359–378.
- Erkorkmaz, K. and Altintas, Y. (2001). High speed CNC system design. part I: jerk limited trajectory generation and quintic spline interpolation. *Machine Tools and Manufacture*, **41**: 1323–1345.
- Espiau, B., Chaumette, F. and Rives, P. (1992). A new approach to visual servoing in robotics. *IEEE Transactions on Robotics and Automation*, **8**(3): 313–326.
- Fakhry, H. and Wilson, W. (1996). A modified resolved acceleration controller for position-based visual servoing. *Mathematical Computer Modelling*, **24**(5/6): 1–9.
- Fleisig, R. and Spence, A. (2001). A constant feed and reduced angular acceleration interpolation algorithm for multi-axis machining. *Computer-Aided Design*, **33**: 1–15.
- Fu, K. and Mills, J. (2005). A planar parallel manipulator—dynamics revisited and controller design. *Proceedings of the International Conference on Intelligent Robots and Systems (IROS'05)*, Edmonton, Canada, 2005, pp. 456–461.
- Gautier, M. and Pognet, P. (2001). Extended Kalman filtering and weighted least squares dynamic identification of robot. *Control Engineering Practice*, **9**(12): 1361–1372.
- Geldart, M., Webb, P., Larsson, H., Backstrom, M., Gindy, N. and Rask, K. (2003). A direct comparison of the machining performance of a variax 5 axis parallel kinetic machining centre with conventional 3 and 5 axis machine tools. *International Journal of Machine Tools and Manufacture*, **43**(11): 1107–1116.
- Ginhoux, R., Gangloff, J., de Mathelin, M., Soler, L., Arenas Sanchez, M. and Marescaux, J. (2004). Beating heart tracking in robotic surgery using 500 Hz visual servoing, model predictive control and an adaptive observer. *Proceedings of the IEEE International Conference on Robotics and Automation (ICRA'04)*, April 2004, pp. 274–279.
- Gogu, G. (2004). Fully-isotropic T3R1-type parallel manipulators. *On Advances In Robot Kinematics*, Lennarčič, J. and Roth, B. (eds). Dordrecht, Kluwer, pp. 265–272.
- Guegan, S., Khalil, W. and Lemoine, P. (2003). Identification of the dynamic parameters of the Orthoglide. *Proceedings of the IEEE International Conference on Robotics and Automation (ICRA'03)*, Taipei, Taiwan, pp. 3272–3277.
- Honegger, M., Brega, R. and Schweitzer, G. (2000). Application of a non-linear adaptive controller to a 6 DOF parallel manipulator. *Proceedings of the IEEE International Conference on Robotics and Automation (ICRA'00)*, San Francisco, CA, pp. 1930–1935.
- Husty, M. (1994). An algorithm for solving the direct kinematics of the Gough–Stewart platforms. *Technical Report TR-CIMS-94-7*, McGill University, Montréal, Canada.
- Hutchinson, S., Hager, G. and Corke, P. (1996). A tutorial on visual servo control. *IEEE Transactions on Robotics and Automation*, **12**(5): 651–670.
- Khalil, W. and Dombre, E. (2002). *Modeling, Identification and Control of Robots*. London, Hermes Penton.
- Khalil, W. and Ibrahim, O. (2004). General solution for the dynamic modeling of parallel robots. In *Proceedings of the IEEE International Conference on Robotics and Automation (ICRA'04)*, New Orleans, LA, 2004, pp. 3665–3670.
- Kim, H. S., Cho, Y. M. and Lee, K.-I. (2005). Robust nonlinear task space control for 6 DOF parallel manipulator. *Automatica*, **41**: 1591–1600.
- Kino, H., Cheah, C., Yabe, S., Kawamura, S. and Arimoto, S. (1999). A motion control scheme in task oriented coordinates and its robustness for parallel wire driven systems. *Proceedings of the International Conference on Advanced Robotics (ICAR'99)*, Tokyo, Japan, 1999, pp. 545–550.
- Kock, S. and Shimacher, W. (2000a). Control of a fast parallel robot with a redundant chain and gearboxes: experimental results. *Proceedings of the International Conference on Robotics and Automation (ICRA'00)*, San Francisco, CA, 2000, pp. 1924–1929.
- Kock, S. and Shimacher, W. (2000b). A mixed elastic and rigid-body dynamic model of an actuation redundant parallel robot with high-reduction gears. *Proceedings of the International Conference on Robotics and Automation (ICRA'00)*, San Francisco, CA, pp. 1918–1923.
- Lambrechts, P., Boerlage, M. and Maarten, S. (2005). Trajectory planning and feedforward design for electromechanical motion systems. *Control Engineering Practice*, **13**: 145–157.
- Lee, S., Song, J., Choi, W. and Hong, D. (2003). Position control of a Stewart platform using inverse dynamics control with approximate dynamics. *Mechatronics*, **13**: 605–619.
- Liu, X., Jin, Z. and Gao, F. (2000). Optimum design of 3-dof spherical parallel manipulators with respect to the conditioning and stiffness indices. *Mechanism and Machine Theory*, **35**: 1257–1267.
- Luh, J., Walker, M. and Paul, R. (1980). Resolved acceleration control of mechanical manipulators. *IEEE Transactions on Automatic Control*, **25**(3): 468–474.
- Marquet, F., Company, O., Krut, S. and Pierrot, F. (2002). Enhancing parallel robot with redundant sensors. *Proceedings of the International Conference on Robotics and Automation (ICRA'02)*, Washington, DC, pp. 4114–4119.
- Marquet, F., Krut, S., Company, O. and Pierrot, F. (2001). Archi: a redundant parallel mechanism—modeling, control and first results. *Proceedings of the International Conference on Intelligent Robots and Systems (IROS'01)*, Maui, HI, pp. 183–188.
- Merlet, J. (1990). An algorithm for the forward kinematics of general 6 DOF parallel manipulator. *Research Report RR 1331*, INRIA, France.
- Merlet, J. (2000). *Parallel robots*. Dordrecht, Kluwer.

- Merlet, J. (2002). Still a long way to go on the road for parallel mechanisms. *Proceedings of the ASME 27th Biennial Mechanisms and Robotics Conference*, Montreal, Quebec, 2002.
- Merlet, J. (2004). Solving the forward kinematics of Gough-type parallel manipulator with interval analysis. *The International Journal of Robotics Research*, **23**: 221–235.
- Nabat, V., de la O Rodriguez, M., Company, O., Krut, S. and Pierrot, F. (2005). Par4: very high speed parallel robot for pick-and-place. *Proceedings of the International Conference on Intelligent Robots and Systems (IROS'05)*, Edmonton, Canada, pp. 1202–1207.
- Newman, W., Birkhimer, C., Horning, R. and Wilkey, A. (2000). Calibration of a Motoman P8 robot based on laser tracking. *Proceedings of the IEEE International Conference on Robotics and Automation (ICRA'00)*, San Francisco, CA, 2000, pp. 3597–3602.
- Oen, K. and Wang, L. (2007). Optimal dynamic trajectory planning for linearly actuated platform type parallel manipulators having task space redundant degree of freedom. *Mechanism and Machine Theory*, **42**(7): 727–750.
- Olsen, M. and Peterson, H. (2001). A new method for estimating parameters of a dynamic robot model. *IEEE Transactions on Robotics and Automation*, **17**(1): 95–100.
- Ouyang, P., Zhang, W. and Xu, F. (2002). Non linear PD control for trajectory tracking with consideration of the design for control methodology. *Proceedings of the International Conference on Robotics and Automation (ICRA'02)*, Washington, DC, pp. 4126–4131.
- Paccot, F., Andreff, N. and Martinet, P. (2007). Revisiting the major dynamic control strategies of parallel robots. *Proceedings of the European Control Conference (ECC)*, Kos, Greece, 2007.
- Paccot, F., Andreff, N., Martinet, P. and Khalil, W. (2006). Vision-based computed torque control for parallel robots. *Proceedings of the 32nd Annual Conference of the IEEE Industrial Electronics Society*, Paris, France, 2006, pp. 3851–3856.
- Pritschow, G. (2002). Influence of the dynamic stiffness on the accuracy of PKM. *Proceedings of the Chemnitz Parallel Kinematic Seminar*, Chemnitz, Germany, 2002, 313–333.
- Renaud, P., Vivas, A., Andreff, N., Poignet, P., Martinet, P., Pierrot, F. and Company, O. (2006). Kinematic and dynamic identification of parallel mechanisms. *Control Engineering Practice*, **14**: 1099–1109.
- Rizk, R., Andreff, N., Fauroux, J., Lavest, J. and Gogu, G. (2006). Precision study of a decoupled four degrees of freedom parallel robot including manufacturing and assembling errors. *Proceedings of the International Conference on Integrated Design and Manufacturing in Mechanical Engineering (IDMME)*, Grenoble, France, 2006.
- Swevers, J., Ganseman, C., Tüekel, B., De Schutter, J. and Van Brussel, H. (1997). Optimal robot excitation and identification. *IEEE Transactions on Robotics and Automation*, **13**(5): 730–740.
- Terrier, M., Dugas, A., and Hascoët, J. (2004). Qualification of parallel kinematics machines in high speed milling on free form. *International Journal of Machine Tools and Manufacture*, **44**: 865–877.
- Thusty, J., Ziegert, J. and Ridgeway, S. (1999). Fundamental comparison of the use of serial and parallel kinematics for machine tools. *Annals of the CIRP*, **48**(1): 351–356.
- Tsai, L. (2000). Solving the inverse dynamics of a Stewart–Gough manipulator by the principle of virtual work. *ASME Journal of Mechanical Design*, **122**: 3–9.
- Vivas, A., Poignet, P. and Pierrot, F. (2003). Predictive functional control for a parallel robot. *Proceedings of the IEEE International Conference on Intelligent Robots and Systems (IROS'03)*, pp. 2785–2790.
- Waldron, K. and Hunt, K. (1991). Series–parallel dualities in actively coordinated mechanisms. *International Journal of Robotics Research*, **10**(2): 473–480.
- Wang, J. and Masory, O. (1993). On the accuracy of a Stewart platform—part I: the effect of manufacturing tolerances. *Proceedings of the IEEE International Conference on Robotics and Automation (ICRA'93)*, Atlanta, GA, pp. 114–120.
- Weiss, L., Sanderson, A. and Neuman, C. (1987). Dynamic sensor-based control of robots with visual feedback. *IEEE Journal of Robotics and Automation*, **3**(5): 404–417.
- Yamane, K., Okada, M., Komine, N. and Nakamura, Y. (1998). Parallel dynamics computation and  $H_\infty$  acceleration control of parallel manipulators for acceleration display. *Proceedings of the International Conference on Robotics and Automation (ICRA'98)*, Leuven, Belgium, pp. 2301–2308.
- Yang, Z. and Huang, T. (2006). Parameter identification and tuning of the servo system of a 3-hss parallel kinematic machine. *International Journal of Advanced Manufacturing Technology*, **31**(5-6): 621–628.
- Zein, M., Wenger, P. and Chablat, D. (2006). Singular curves and cusp points in the joint space of 3-RPR parallel manipulators. *Proceedings of the IEEE International Conference on Robotics and Automation (ICRA'06)*, Orlando, FL, pp. 777–782.
- Zhiyong, Y. and Huang, T. (2004). A new method for tuning PID parameters of a 3-DOF reconfigurable parallel kinematic machine. *Proceedings of the IEEE International Conference on Robotics and Automation (ICRA'04)*, New Orleans, LA, pp. 2249–2254.